iScience

CellPress
OPEN ACCESS

Article

Possible involvement of a MEG3-miR-21-SPRY1-NF-κB feedback loop in spermatogenic cells proliferation, autophagy, and apoptosis

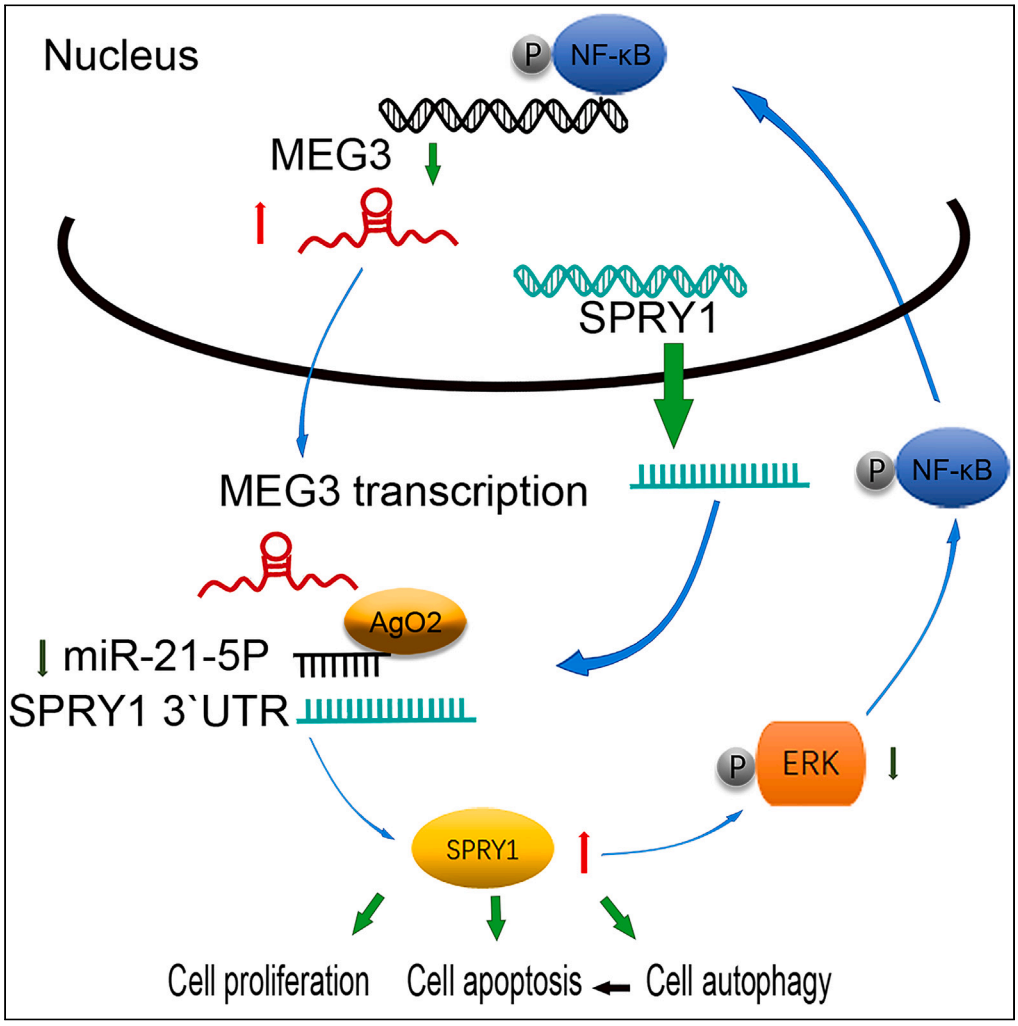

Xingyu Fang, Xiaotong Lu, Yujie Ma, ..., Haoran Guo, Haosen Xiong, Wenyan Song

csxokgzr@sina.com

Highlights

MEG3 was highly expressed in spermatids and spermatogonia in NOA

MEG3 inhibited proliferation, promoted autophagy, and apoptosis *in vitro* and *in vivo*

MEG3 functioned through miR-21/SPRY1/ERK in NT-2 cells

A positive feedback loop between MEG3 and SPRY1 presumably existed

Fang et al., iScience 27, 110904
October 18, 2024
https://doi.org/10.1016/j.isci.2024.110904

iScience

CellPress
OPEN ACCESS

Article

Possible involvement of a MEG3-miR-21-SPRY1-NF-κB feedback loop in spermatogenic cells proliferation, autophagy, and apoptosis

Xingyu Fang,[1,4] Xiaotong Lu,[1,4] Yujie Ma,[1,4] Ning Sun,[1] Yunyun Jiao,[1] Hui Meng,[2] Mengjiao Song,[1] Haixia Jin,[1] Guidong Yao,[1] Ning Song,[1] Zhaoting Wu,[1] Shuang Wen,[1] Haoran Guo,[3] Haosen Xiong,[2] and Wenyan Song[1,5,*]

SUMMARY

Non-obstructive azoospermia (NOA) is the most incurable form of male infertility with a complex etiology. Long non-cording RNAs (lncRNAs) were associated with regulating spermatogenesis. Herein, differentially expressed lncRNAs between NOA and control male were screened by RNA-seq analysis. MEG3 was upregulated in NOA tissues and inhibited cell proliferation and promoted cell autophagy and apoptosis *in vitro*. Through RNA immunoprecipitation (RIP), biotin pull-down assays, and dual-luciferase reporter assays, MEG3 was proved to act as a competing endogenous RNA of microRNA (miR)-21 and thus influenced the SPRY1/ERK/mTOR signaling pathway. Additionally, bioinformatic prediction and chip assay revealed that MEG3 was possibly regulated by nuclear factor κB (NF-κB) and SPRY1/NF-κB/MEG3 formed a feedback loop. Seminiferous tubule microinjection further investigated the effects of MEG3 on testes *in vivo*. These findings demonstrated that MEG3-miR-21-SPRY1-NF-κB probably acted as a feedback loop leading to azoospermia. Our study might provide a target and theoretical basis for diagnosing and treating NOA.

INTRODUCTION

Infertility is an emerging global health problem among married couples, which troubles about 15% of reproductive couples.[1,2] Thirty to fifty percent of infertility cases attribute to abnormality of male.[3,4] Azoospermia, defined as the complete absence of sperm from the twice ejaculate semen analysis, can be classified into obstructive azoospermia (OA) and non-obstructive azoospermia (NOA) according to the etiology.[5] OA accounts for 40% and is characterized by an obstruction in the ductal system at any point along the male genital tract.[6,7] Conversely, NOA occurs as a consequence of impaired spermatogenesis.[8] Developing intracytoplasmic sperm injection (ICSI) has opened a new epoch in assisted reproduction. It is the main treatment means for male patients with infertility. Through conventional or microscopic testicular sperm extraction (TESE), sperm can be retrieved in almost all cases of OA but only in 50% of NOA.[9] Consequently, there is an urgent clinical demand for alternate treatments for NOA that would repair testicular damage or allow the production of spermatozoa.

Spermatogenesis is affected by several genetic and environmental factors. This process is governed by the parallel and serial function of a large number of genes in spermatogenic cells.[10] Accurate control of gene expression is a prerequisite for normal spermatogenesis.[11] Genetic factors have been used as part of the routine diagnostic workup of infertile men. However, the diagnostic yield of NOA with primary testicular failure remains low.[12] With the optimization of sequencing technologies, high-throughput sequencing is used for studying NOA.[13] Some noncoding RNAs (ncRNAs) are verified responsible for posttranscriptional gene regulation throughout spermatogenesis.[14,15] Long noncoding RNAs (lncRNAs) are a class of ncRNA, which are longer than ~200 nucleotides in length and play essential roles in human diseases through interacting with DNA, RNA, protein molecules, or their combinations.[16] lncRNAs broadly participate in various biological functions and can regulate the expression of target genes at transcriptional,[17] post-transcriptional,[18] and epigenetic levels.[19,20] Many lncRNAs have been reported to function in spermatogenesis and male infertility.[21] Rolland et al. identified 113 known lncRNAs, and 20 novel genes were important for spermatogenesis.[22] Lü et al. found that NLC1-C accumulated in the nucleus of spermatogonia and primary spermatocytes in the testis, repressed miR-320a and miR-383 transcripts by binding to nucleolin, and led to infertility.[23] Genomic studies on azoospermia have been performed to profile the mutational landscape of the OA and NOA.[24,25] However, the specific functions of lncRNAs in NOA patients remain unclear.

[1]Center for Reproductive Medicine, The First Affiliated Hospital of Zhengzhou University, Zhengzhou 450052, China
[2]Department of Pathology, The First Affiliated Hospital of Zhengzhou University, Zhengzhou 450052, China
[3]School of Basic Medical Sciences, Academy of Medical Sciences, Zhengzhou University, Zhengzhou, China
[4]These authors contributed equally
[5]Lead contact
*Correspondence: csxokgzr@sina.com
https://doi.org/10.1016/j.isci.2024.110904

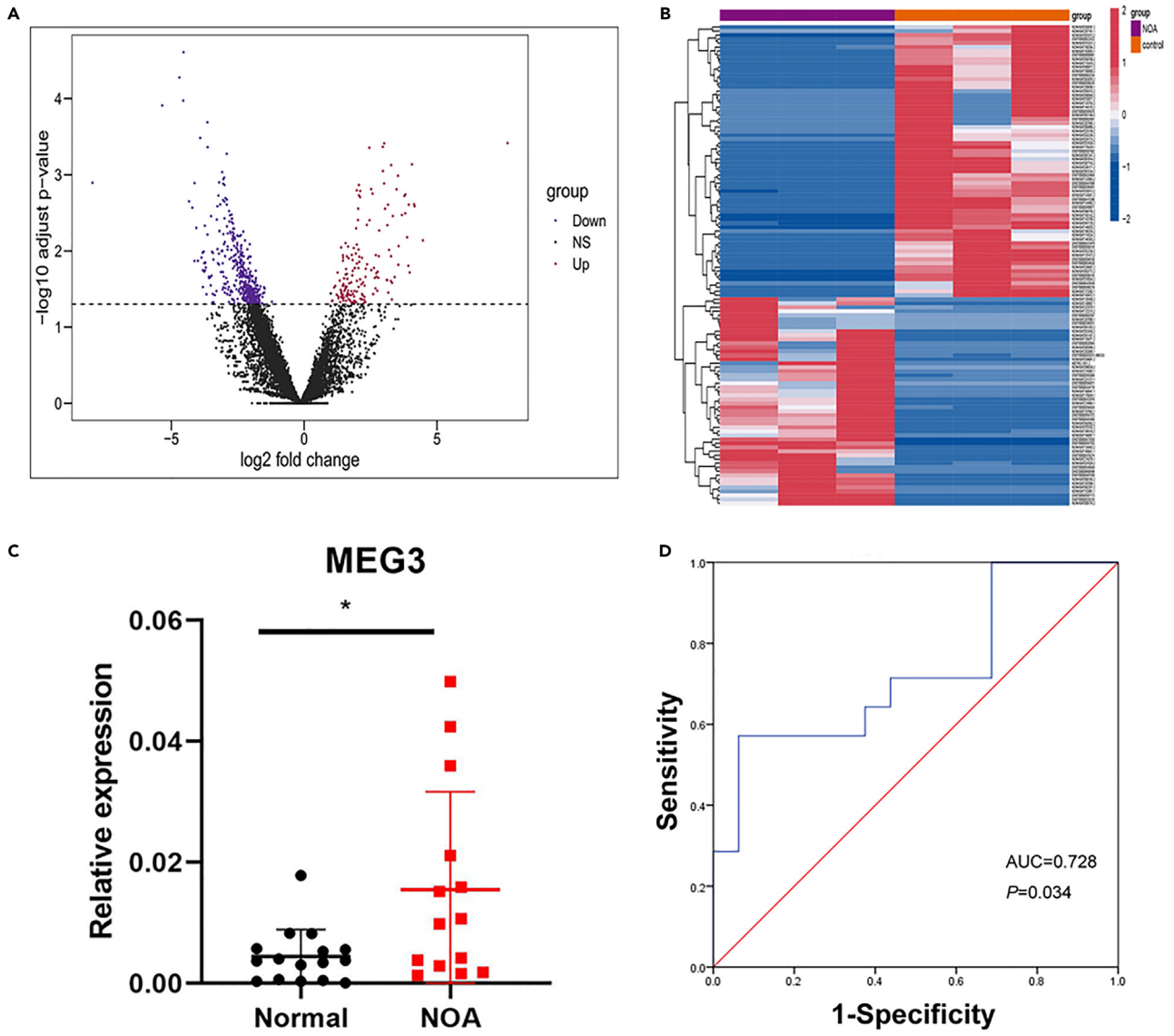

Figure 1. RNA-seq and expression of lncRNA MEG3 in testicular tissues of NOA patients

(A) The volcano plot showed differentially expressed lncRNAs in tissues from patients with NOA and those with normal spermatogenesis. Red dots indicated upregulated lncRNAs, and purple dots indicated downregulated lncRNAs.

(B) The heatmap of differentially expressed lncRNAs. The red color on the side of the row represented the upregulated lncRNAs in NOA patients, whereas the blue color represented downregulated lncRNAs.

(C) qPCR detection showed MEG3 expression in testicular tissues.

(D) ROC analysis of MEG3 to predict NOA. ROC, receiver operating characteristic. Data are represented as mean ± SD; *$p < 0.05$; **$p < 0.01$; ***$p < 0.001$, ****$p < 0.0001$.

LncRNAs can regulate autophagy by targeting autophagy-related proteins.[26] HOTAIR (HOX transcript antisense RNA) is intimately implicated in tumorigenesis, mediating chromosome remodeling and collaborating with multi-comb inhibition complex 2 (polycomb repressive complex 2 [PRC2]) to regulate gene expression in various biological processes.[27] In hepatocellular carcinoma, HOTAIR can activate autophagy by promoting the expression of ATG3 and ATG7.[28] In papillary thyroid carcinoma (PTC), the expression level of BRAF-activated noncoding RNA (BANCR) is significantly elevated, which helps PTC cells proliferate and activate autophagy.[28] However, few reports on regulating autophagy by lncRNAs in spermatogenesis exist. Therefore, our study explored whether the effects of lncRNAs on spermatogenesis in NOA is due to autophagy.

Numerous studies have shown that lncRNAs functioned as competing endogenous RNAs (ceRNAs) to influence mRNA or other lncRNA transcripts by competitively binding to miRNA response elements (MREs).[29,30] miRNAs are a class of small noncoding RNAs with

Table 1. Clinicopathological features of all patients

Features	NOA group	Control group	*p* value
Number (n)	14	16	
Age (years)	31.93 ± 7.498	31.44 ± 4.816	0.836
FSH (IU/L)	12.9292 ± 8.878	3.8620 + 2.083	0.005[a]
LH (IU/L)	5.6275 ± 2.832	4.0507 ± 1.848	0.101
T (g/mL)	3.83 (3.16–6.54)	3.39 (2.31–4.21)	0.504
PRL (ng/mL)	12.9989 ± 8.15	11.0079 ± 5.00	0.474
E2 (pg/mL)	37.02 (24.47–47.50)	26.14 (21.38–31.73)	0.037[a]
P (ng/mL)	0.21 (0.20–0.30)	0.19 (0.16–0.31)	0.596
Volume of left testis (mL)	10.8 (8.6–12.0)	12.5 (12.0–15.0)	0.011[a]
Volume of right testis (mL)	10.7 (6.5–12.5)	13.1 (12.0–15.2)	0.006[a]

[a]$p < 0.05$.

approximately 22 nucleotides that are involved in regulating spermatogenesis during mitotic, meiotic, and post-meiotic stages.[11,31,32] Mature miRNAs repress translation and cause mRNA degradation through loading into the RNA-induced silencing complex (RISC).[33] Researches have shown that MEG3 (maternally expressed 3) acted as a sponge for miR-21 to play role in the regulation of many diseases such as non-small cell lung cancer,[34] endometriosis,[35] melanoma,[36] non-alcoholic fatty liver disease,[37] and preeclampsia.[38] Our study revealed that MEG3 was highly expressed in NOA. Therefore, whether MEG3 acted as a sponge for miR-21 and participated in regulating the function of spermatogenic cells in NOA remains unclear.

The SPRY1 (sprouty RTK signaling antagonist 1) is known to be a member of the Sprouty family, which can negatively regulate the receptor tyrosine kinases (RTKs) signaling pathway and participate in biological processes such as organ development and disease occurrence.[39] Present studies focused on cancers and renal fibrosis and myocardial dysfunction find that SPRY1 is one of the target gene of miR-21.[40–44] However, report on the correlation between SPRY1 and human sperm production remains absent.

Herein, RNA sequencing (RNA-seq) was used to analyze differential gene expression of the testicular tissues in patients with NOA. The lncRNA MEG3 was found to be significantly upregulated in testicular tissues of patients with NOA. Subsequently, the regulatory relationship between lncRNA MEG3-miR-21-SPRY1-NF-κB (nuclear factor κB) was determined using molecular biology experiments in human NTERA-2 cells and mouse models. Finally, the effects of lncRNA MEG3-miR-21-SPRY1-NF-κB feedback loop on the proliferation, autophagy, and apoptosis in spermatogenic cells were evaluated by functional experiments. Our study provides insights into NOA pathogenesis and offers potential treatment options for this condition.

RESULTS

RNA-seq and expression of lncRNA MEG3 in testicular tissues of NOA patients

Herein, we performed whole-genome transcriptome profiling by RNA sequencing to explore differentially expressed genes between patients with NOA and normal spermatogenesis. Validation of sequencing results by qPCR is shown in Figure S1. Volcano plots showed that 161 lncRNAs were upregulated, whereas 505 lncRNAs were downregulated in NOA (Figure 1A). lncRNA-MEG3 was one of the highly expressed lncRNAs in the NOA group (Figure 1B). To further confirm MEG3 expression, we assessed it in 14 NOA and 16 control testicular tissues. Table 1 illustrated the clinicopathologic features of 30 patients. Subsequently, we observed no significant differences in age, serum testosterone (T), serum prolactin (PRL), and progesterone (P) ($p > 0.05$). Estradiol (E2) (37.02 [24.47–47.50] vs. 26.14 [21.38–31.73]) and serum follicle-stimulating hormone (FSH) (12.9292 ± 8.878 vs. 3.8620 + 2.083, $p < 0.05$) levels in the NOA group were significantly higher than those in the control group, with decreasing volume of right (10.7 [6.5–12.5] vs. 13.1 [12.0–15.2], $p = 0.006$) and left (10.8 [8.6–12.0] vs. 12.5 [12.0–15.0]; $p = 0.011$) testis. The qPCR results further demonstrated that the MEG3 expression levels were significantly higher in NOA tissues (Figure 1C). Diagnostic significance of MEG3 in distinguishing NOA from control patients was determined by ROC curve analysis (area under the curve [AUC] = 0.808; $p < 0.05$) (Figure 1D).

LncRNA MEG3 inhibited proliferation and promoted autophagy and apoptosis of spermatogenic cells *in vitro* and *in vivo*

Consequently, we investigated the role of MEG3 by silencing or overexpressing it in NT-2 cells. Figures 2A and S2A illustrated that MEG3 knockdown significantly enhanced cell vitality and promoted the proliferation of NT-2 cells, whereas MEG3 overexpression inhibited proliferation. MEG3 overexpression significantly elevated the LC3II: LC3I ratio and beclin-1 levels, whereas MEG3 knockdown exerted the opposite effect, indicating that MEG3 promoted autophagy (Figure 2C). Tandem-labeled GFP-mRFP-LC3 was transfected into cells to monitor autophagy maturation. Consequently, we observed that MEG3 overexpression significantly increased the yellow and red puncta, and MEG3 knockdown decreased them, revealing that MEG3 function on autophagosome accumulation was mainly due to the impairment of autophagic degradation in NT-2 cells (Figure 2D).

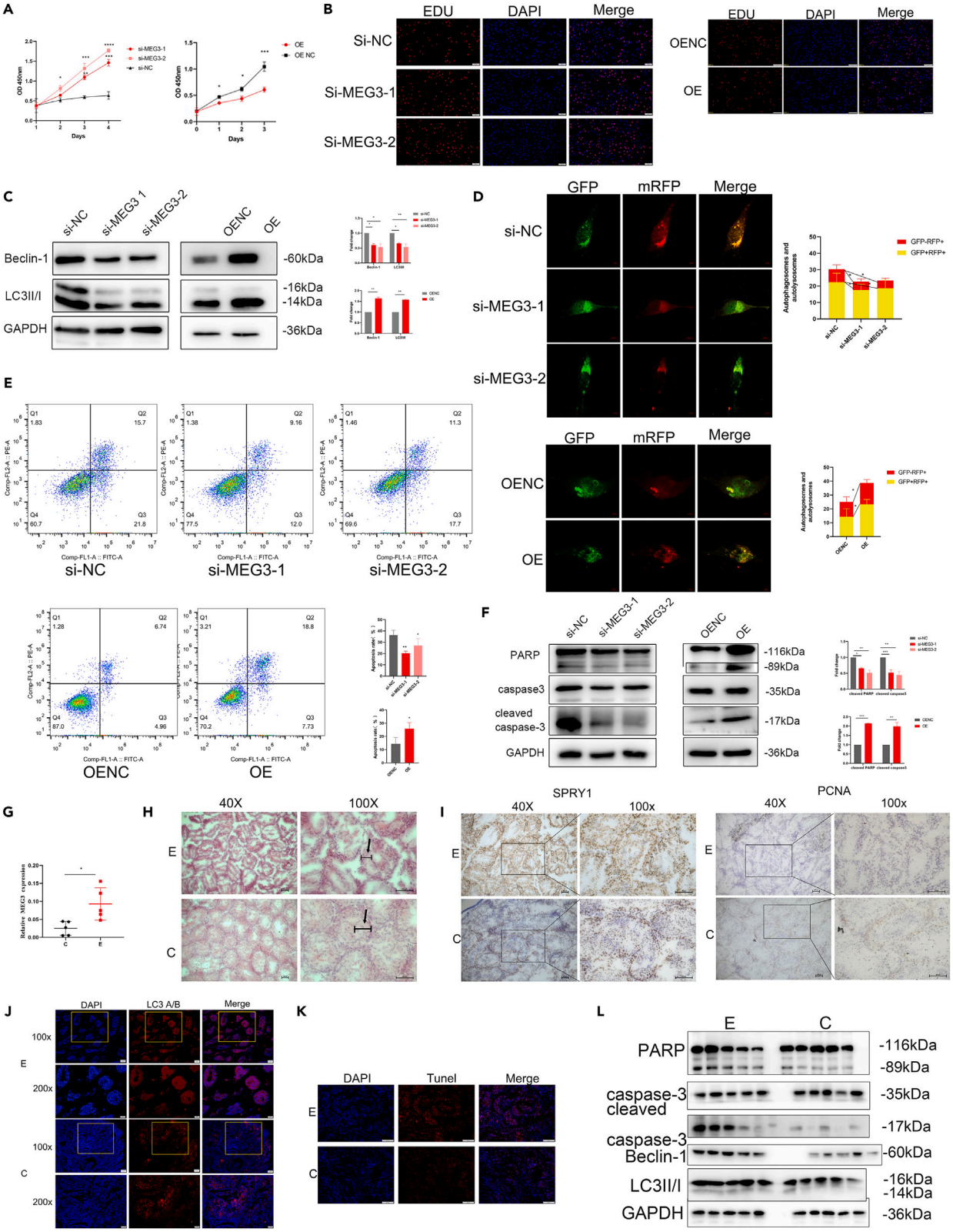
A
si-MEG3-1
si-MEG3-2
si-NC
OE
OE NC
OD 450nm
Days
B
EDU
DAPI
Merge
Si-NC
Si-MEG3-1
Si-MEG3-2
OENC
OE
C
si-NC
si-MEG3 1
si-MEG3-2
OENC
OE
Beclin-1
LC3II/I
GAPDH
-60kDa
-16kDa
-14kDa
-36kDa
D
GFP
mRFP
Merge
si-NC
si-MEG3-1
si-MEG3-2
OENC
OE
GFP-RFP+
GFP+RFP+
Autophagosomes and autolysosomes
E
si-NC
si-MEG3-1
si-MEG3-2
OENC
OE
Comp-FL2-A :: PE-A
Comp-FL1-A :: FITC-A
F
si-NC
si-MEG3-1
si-MEG3-2
OENC
OE
PARP
caspase3
cleaved caspase-3
GAPDH
-116kDa
-89kDa
-35kDa
-17kDa
-36kDa
G
Relative MFG3 expression
C
E
H
40X
100X
E
C
I
SPRY1
PCNA
40X
100x
E
C
J
DAPI
LC3 A/B
Merge
100x
200x
E
C
K
DAPI
Tunel
Merge
E
C
L
E
C
PARP
caspase-3 cleaved
caspase-3
Beclin-1
LC3II/I
GAPDH
-116kDa
-89kDa
-35kDa
-17kDa
-60kDa
-16kDa
-14kDa
-36kDa

Figure 2. LncRNA MEG3 inhibited proliferation and promoted autophagy and apoptosis of germ cells *in vitro* and *in vivo*

(A) CCK-8 assays were performed to determine the viability of NT-2 cells.

(B) Representative images of EDU assay.

(C) Western blotting was conducted to verify the protein expression of LC3 II/1 and beclin-1 in NT-2 cells.

(D) Autophagy flow in NT-2 cells was observed by confocal microscopy. Scale bar = 5 μm (confocal microscopy).

(E) Annexin V-FITC-PI analysis of cell apoptosis in NT-2 cells. Representative scatterplots and quantitative results are shown.

(F) Western blot analysis of cleaved caspase-3 and cleaved RARP expression (left) and gray analysis normalized to GAPDH (right).

(G) RT-qPCR analysis of the mouse homologous gene of MEG3 in MEG3-AAV9 group (E) and negative control-AAV9 group (C).

(H) Testicular sections stained with H&E.

(I) Representative IHC staining of PCNA and SPRY1 in the testis. Scale bar = 100 μm.

(J) Immunostaining of testis paraffin section for LC3 A/B (red). Nuclei were stained with DAPI (blue). Scale bar was marked on the figure.

(K) Representative staining images of TUNEL assay on testis sections. Scale bar = 200 μm

(L) Western blot images of mice testicular tissues. Data were represented as mean ± SD; *$p < 0.05$; **$p < 0.01$; ***$p < 0.001$, ****$p < 0.0001$.

Furthermore, knockdown of MEG3 caused a substantial decrease of apoptosis rate compared with the negative control after treatment with etoposide. Meanwhile, overexpression of MEG3 showed the opposite result (Figure 2E). The MEG3 overexpression promoted the expressions of cleaved caspase-3 and cleaved PARP [poly (ADP-ribose) polymerase 1] after induced by etoposide. Conversely, the MEG3 knockdown yielded contrary results (Figure 2F). These data demonstrated that MEG3 promoted autophagy and apoptosis but inhibited proliferation in NT-2 cells.

Herein, we constructed a microinjection system into seminiferous tubules to further clarify the action of MEG3 *in vivo*. Virus-infected seminiferous tubules were confirmed using RT-qPCR analysis and immunofluorescence (Figures 2G and S2B). MEG3 was overexpressed for 1 week after the microinjection. Subsequently, we examined the morphology of testicular tissues using H&E-stained sections to identify the phenotypes of testes with upregulated MEG3 expression. Morphologic change and seminiferous tubular cell loss were observed in testes with upregulated MEG3. Notably, the thickness of the seminiferous epithelium was substantially reduced, indicating decreased numbers and impaired spermatogenic cell function (Figure 2H).

Consequently, we detected PCNA (proliferating cell nuclear antigen) to assess the proliferation. Immunohistochemistry (IHC) results revealed that PCNA was downregulated in testes with upregulated MEG3 compared with that in the negative control testes (Figure 2I). These findings indicated that MEG3 inhibited germ cell proliferation. Given the functional roles of MEG3 in autophagy and apoptosis *in vitro*, we conducted GFP-LC3 immunofluorescence analysis to assess autophagosome formation. The results showed that the number of GFP-LC3 puncta was significantly increased in MEG3 overexpression group (E) compared with the negative control group (C) (Figures 2J and S2C). The protein levels of Beclin-1 and the LC3 II/I ratio were also increased in testicular tissues with MEG3 overexpression (Figures 2L and S2E).

Furthermore, we investigated the rate of germ cell apoptosis in testicular tissues with upregulated MEG3 through TUNEL assay. A significant increase in the number of apoptotic cells was detected in the testes with upregulated MEG3 expression (Figures 2K and S2D). The expression levels of cleaved caspase-3 and cleaved PARP showed the same trend (Figures 2L and S2E). These *in vivo* data revealed that MEG3 contributed to the impairment of spermatogenesis by promoting autophagy and apoptosis and inhibiting proliferation in germ cells.

MEG3 acted as a competing endogenous RNA sponged for miR-21 in NT-2 cells

We examined the location of MEG3 in testicular tissues and NT-2 cell lines through FISH. Interestingly, we observed that MEG3 was presented in spermatogenic and Sertoli cells. Furthermore, MEG3 was expressed in the cytoplasm and nucleus of NT-2 cells (Figure 3A). Single-cell RNA-seq analysis of normal human testicles of GSE106487 showed that MEG3 dominatingly expressed in spermatid cells, few in Sertoli cells. Analysis of single-cell sequencing dataset GSE149512 showed MEG3 was overexpressed in spermatogonia, spermatids, and Sertoli cells in patients with NOA (Figure 3B). Moreover, bioinformatic prediction showed overlapped miRNAs in the miRcode and LncBase databases (Figure 3C). Furthermore, we analyzed the GSE45887 cohort and detected that miR-21 was one of the most downregulated miRNAs in NOA testicular tissues among these miRNAs (Figure 3D). To dissect the underlying mechanism of MEG3, we performed RNA pull-down assay to verify that miR-21 was pulled down by bio-MEG3, indicating that MEG3 could bind to miR-21 directly (Figure 3E). Moreover, RNA immunoprecipitation (RIP) results disclosed that the MEG3 amount pulled down with the AGO2 antibody was significantly increased in the miR-21 mimics group compared with the IgG group, indicating that MEG3 was likely in the miR-21 RISC complex (Figure 3F). The findings of the dual-luciferase reporter assay revealed that miR-21 mimics significantly reduced the luciferase activity of MEG3-WT but not that of MEG3-MUT, verifying that MEG3 could directly interact with miR-21 (Figure 3G).

Similarly, MEG3 knockdown significantly increased miR-21 expression in NT-2 cells, whereas MEG3 overexpression inhibited miR-21 (Figure 3H). Briefly, these data demonstrated that MEG3 directly interacted with miR-21.

MiR-21 promoted spermatogenic cell proliferation and suppressed autophagy and apoptosis by targeting and regulating SPRY1

For most miRNA, matching with the 3′ UTR of mRNA is required for mediating post-transcriptional control.[45] Bioinformatics analysis using forecasting software, including miRDB, Starbase, and TargetScan, showed that SPRY1 possessed a binding site for miR-21 (Figure S3). The luciferase assay results showed that the fluorescence intensity of the SPRY1-wt and miR-21 co-transfection group was significantly lower

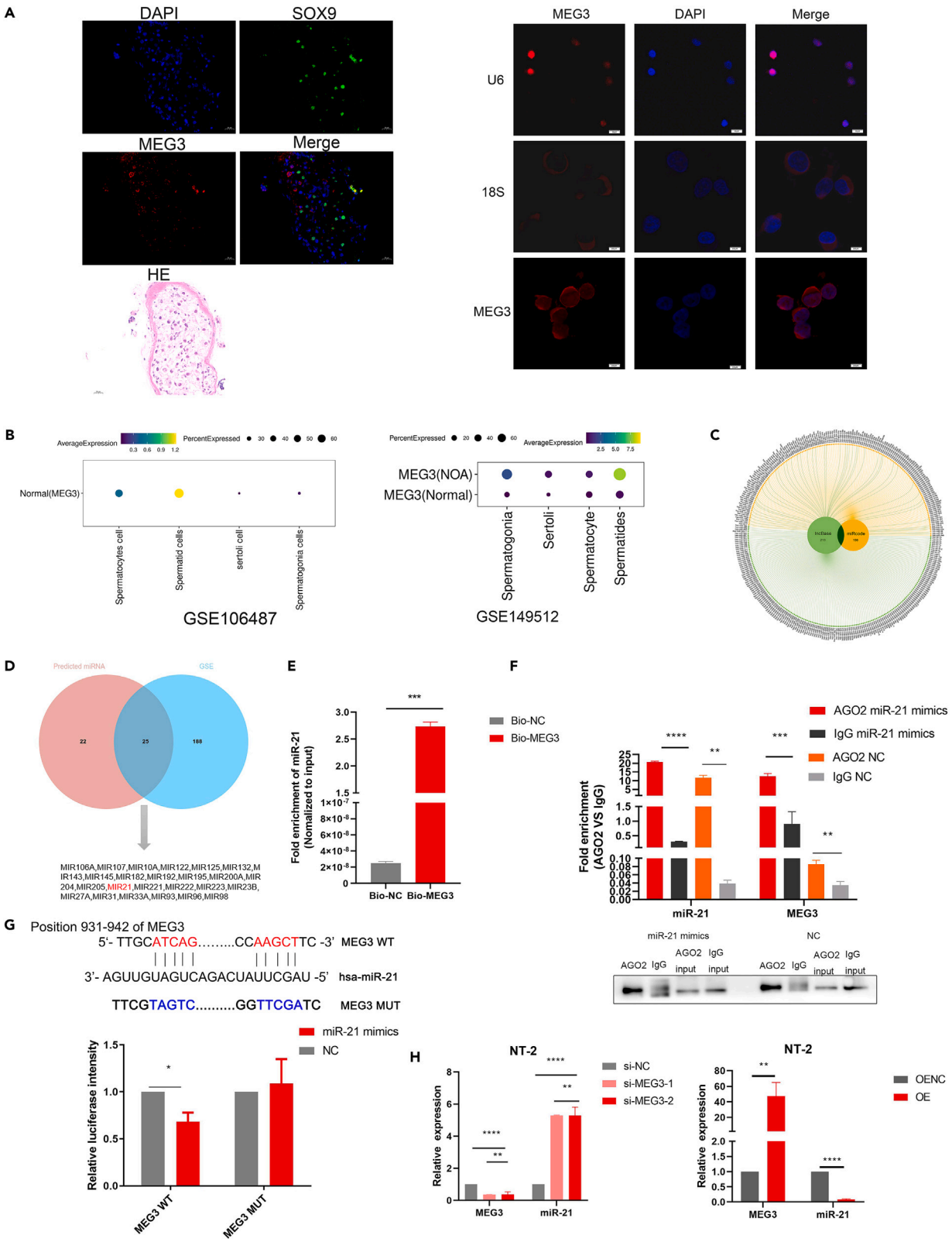
A
DAPI
SOX9
MEG3
Merge
HE
MEG3
DAPI
Merge
U6
18S
MEG3
B
AverageExpression
PercentExpressed
Normal(MEG3)
Spermatocytes cell
Spermatid cells
sertoli cell
Spermatogonia cells
GSE106487
PercentExpressed
AverageExpression
MEG3(NOA)
MEG3(Normal)
Spermatogonia
Sertoli
Spermatocyte
Spermatides
GSE149512
C
D
Predicted miRNA
GSE
22
25
188
MIR106A,MIR107,MIR10A,MIR122,MIR125,MIR132,MIR143,MIR145,MIR182,MIR192,MIR195,MIR200A,MIR204,MIR205,MIR21,MIR221,MIR222,MIR223,MIR23B,MIR27A,MIR31,MIR33A,MIR93,MIR96,MIR98
E
Fold enrichment of miR-21 (Nomalized to input)
Bio-NC
Bio-MEG3
F
Bio-NC
Bio-MEG3
AGO2 miR-21 mimics
IgG miR-21 mimics
AGO2 NC
IgG NC
Fold enrichment (AGO2 VS IgG)
miR-21
MEG3
miR-21 mimics
NC
AGO2
IgG
input
G
Position 931-942 of MEG3
5'- TTGCATCAG.....CCAAGCTTC -3' MEG3 WT
3'- AGUUGUAGUCAGACUAUUCGAU -5' hsa-miR-21
TTCGTAGTC.....GGTTCGATC MEG3 MUT
miR-21 mimics
NC
Relative luciferase intensity
MEG3 WT
MEG3 MUT
H
NT-2
si-NC
si-MEG3-1
si-MEG3-2
Relative expression
MEG3
miR-21
NT-2
OENC
OE
Relative expression
MEG3
miR-21

Figure 3. MEG3 acted as a competing endogenous RNA sponged for miR-21 in NT-2 cells

(A) FISH assays identifying the subcellular location of MEG3 in testicular tissues (left) and NT-2 cells (right).

(B) Single-cell RNA sequencing analysis of MEG3 in GSE106487 and GSE149512.

(C) miRNAs overlapped in miRcode and lncBase combined with MEG3.

(D) Intersected miRNA of the GSE45887 cohort and predicted target gene for MEG3.

(E) RNA pull-down assays were used to examine the interaction of MEG3 and miR-21 in NT-2 cells.

(F) RIP with an AGO2 antibody was used to assess the endogenous binding of MEG3 and miR-21 to AGO2 in NT-2 cells, and immunoglobulin G (IgG) was used as the control. MEG3 and miR-21 levels were presented as fold enrichment in Ago2 relative to input. The RIP efficiency of the AGO2 protein was detected by western blot.

(G) Dual luciferase reporter assay was conducted with wild-type and mutant-type luciferase reporter vectors. The relative fluorescence intensity was calculated as Renilla activity/firefly luciferase activity.

(H) Relative expression of miR-21 in NT-2 cells. Data are represented as mean ± SD; *$p < 0.05$; **$p < 0.01$; ***$p < 0.001$, ****$p < 0.0001$.

than that of the SPRY1-mut and miR-21 co-transfection groups (Figure 4A). The results of mRNA and western blot analyses revealed that suppression of miR-21 increased SPRY1 level, whereas miR-21 overexpression induced SPRY1 reduction at RNA and protein levels (Figures 4B and 4C). Proliferation assays indicated that miR-21 downregulation reduced proliferation, whereas miR-21 upregulation promoted proliferation (Figures 4D and 4E).

Additionally, SPRY1 knockdown increased proliferation activity (Figures S4A and S4B). Besides, our results showed that yellow and red puncta were significantly increased by miR-21 inhibitor and decreased by miR-21 mimics in GFP-mRFP-LC3 stably transfected NT-2 cells (Figure 4F). Moreover, we confirmed that miR-21 mimics decreased LC3II:I and beclin-1 expression, whereas the miR-21 inhibitor increased the expression (Figure 4G). Additionally, we observed that si-SPRY1 suppressed autophagy (Figures S3C and S3D). Flow cytometry indicated that the apoptotic rate was notably increased in the miR-21 inhibitor group but decreased in the miR-21 mimics group (Figure 4H). MiR-21 mimics inhibited the expressions of cleaved caspase-3 and cleaved PARP after the induction of apoptosis by etoposide. The miR-21 inhibitor led to the contrary results (Figure 4I). SPRY1 knockdown showed the same trend as miR-21 mimics (Figures S3E and S3F). These results indicated that miR-21 inhibited, while SPRY1 promoted, autophagy and apoptosis in NT-2 cells. Therefore, our data indicated that miR-21 promoted cell proliferation and suppressed cell autophagy and apoptosis by matching with the 3′ UTR of SPRY1 and suppressing its translation.

MEG3 promoted the miR-21 downstream SPRY1 by binding to miR-21

Since MEG3 shares miR-21 binding with 3′ UTR of SPRY1, we wondered whether MEG3 modulated miR-21-mediated inhibition of SPRY1 in NT-2 cells. Consequently, we performed rescue assays to evaluate whether MEG3 regulated SPRY1 by competing for miR-21. Briefly, we overexpressed miR-21 after MEG3 pcDNA3.1 plasmid transfection in NT-2 cells. The results established that MEG3 overexpression induced SPRY1 mRNA and protein levels, which were antagonized by miR-21 mimics. Furthermore, MEG3 knockdown deduced SPRY1 mRNA and protein levels, whereas MEG3 overexpression induced SPRY1 expression (Figures 5A and 5B). Additionally, the IHC result of mouse testicular tissues showed that SPRY1 expression was upregulated in the MEG3 overexpression group (Figure 2I).

The results of CCK-8 and EDU indicated that the effects of MEG3 on proliferation were observably abrogated by miR-21 overexpression in NT-2 cells (Figures 5C and 5D). These results suggested that decreased levels of miR-21 expression were essential for cell proliferation inhibited by MEG3 upregulation. Fluorescence imaging and WB revealed that autophagy was significantly increased in NT-2 cells with high MEG3 expression, whereas miR-21 mimics rescued this effect (Figures 5E and 5F). Concerning the regulation of MEG3 on cell apoptosis, we found that the increased apoptotic of NT-2 cells treated with MEG3 overexpression was abolished by simultaneous miR-21 mimics (Figures 5G and 5H), indicating that the miR-21 level was also essential for the apoptosis of NT-2 cells induced by MEG3 overexpression.

Furthermore, we detected SPRY1 expression in clinical specimens and observed that SPRY1 was upregulated in NOA patients (Figure 5I). Spearman's correlation analysis revealed that SPRY1 expression was positively associated with MEG3 expression in 30 clinical testicular tissues (Figure 5J). The MEG3 inhibited cell proliferation and promoted cell autophagy and apoptosis by modulating the miR-21/SPRY1 axis in NT-2 cells and testicular tissues.

MEG3 promoted apoptosis by enhancing the autophagy of spermatogenic cells through miR-21/SPRY1/ERK pathway

SPRY1 is an essential gene in the canonical ERK (extracellular regulated MAP kinase)/mTOR (mechanistic target of rapamycin kinase) signaling pathway. We sought to determine whether MEG3 regulated ERK/mTOR signaling through miR-21/SPRY1 axis in NT-2 cells. Unsurprisingly, MEG3 knockdown facilitated mTOR and ERK phosphorylation, whereas MEG3 overexpression suppressed it (Figure 6A). The expressions of p-ERK and p-mTOR were also regulated by miR-21 (Figure 6B). Knockdown of SPRY1 attenuated their expression (Figure S4G). Furthermore, rescue assays revealed that MEG3 led to a significant decrease in p-ERK and p-mTOR protein levels, which were counteracted by miR-21 mimics (Figure 6C). The WB results of p-mTOR and p-ERK expression in mouse testicular tissues showed a similar downward trend *in vivo* (Figure 6D).

Herein, we employed ERK inhibitor MEK126 (Selleck) as an autophagy accelerator to further investigate the crosstalk between apoptosis and autophagy. We detected the corresponding expressions of p-ERK, LC3 II/I, and beclin-1 in NT-2 cells after treatment with MEK126 at different concentrations (0, 0.5, 5, 10, 25, and 50 nM, respectively) for 24 h. The findings showed in contrast to the steady level of ERK, the expression of p-ERK showed a downward trend below 25 nM concentrations. However, a simultaneous decline in ERK expression was observed at 50 nM (Figure 6E). Hence, we selected 25 nM as the optimum concentration of MEK162 and treated NT-2 simultaneously

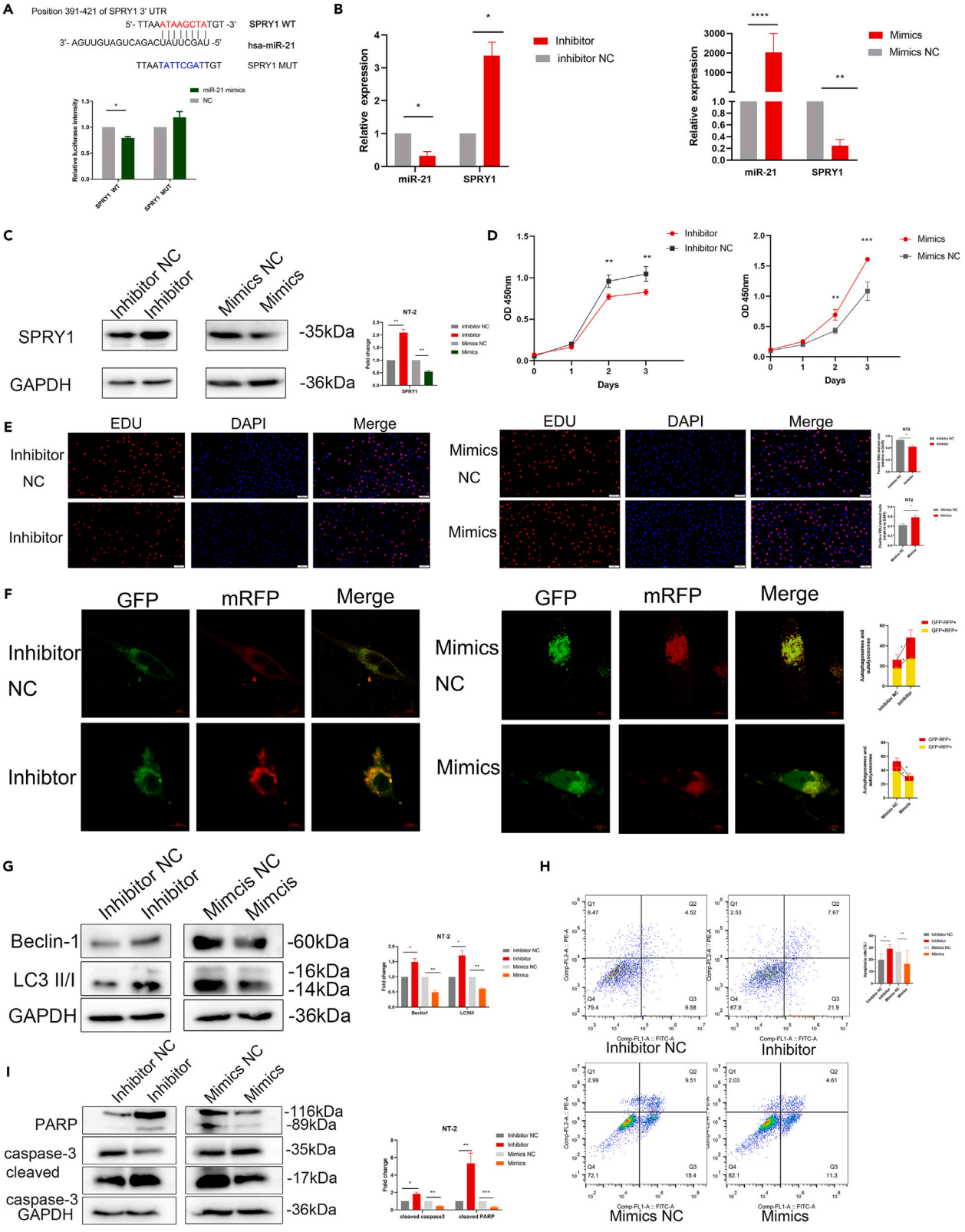
A
Position 391-421 of SPRY1 3' UTR
5'- TTAAATAAGCTATGT -3'
SPRY1 WT
3'- AGUUGUAGUCAGACUAUUCGAU -5'
hsa-miR-21
TTAATATTCGATTGT
SPRY1 MUT
miR-21 mimics
NC
Relative luciferase intensity
SPRY1 WT
SPRY1 MUT
B
Relative expression
Inhibitor
inhibitor NC
miR-21
SPRY1
Relative expression
Mimics
Mimics NC
miR-21
SPRY1
C
Inhibitor NC
Inhibitor
Mimics NC
Mimics
SPRY1
GAPDH
-35kDa
-36kDa
NT-2
Fold change
SPRY1
D
Inhibitor
Inhibitor NC
OD 450nm
Days
Mimics
Mimics NC
OD 450nm
Days
E
EDU
DAPI
Merge
Inhibitor NC
Inhibitor
Mimics NC
Mimics
F
GFP
mRFP
Merge
Inhibitor NC
Inhibtor
Mimics NC
Mimics
G
Inhibitor NC
Inhibitor
Mimcis NC
Mimcis
Beclin-1
LC3 II/I
GAPDH
-60kDa
-16kDa
-14kDa
-36kDa
NT-2
Fold change
Beclin1
LC3II
H
Inhibitor NC
Inhibitor
Mimics NC
Mimics
I
Inhibitor NC
Inhibitor
Mimcs NC
Mimcis
PARP
caspase-3 cleaved
caspase-3
GAPDH
-116kDa
-89kDa
-35kDa
-17kDa
-36kDa
NT-2
Fold change
cleaved caspase3
cleaved PARP

Figure 4. MiR-21 promoted spermatogenic cell proliferation and suppressed autophagy and apoptosis by targeting and regulating SPRY1

(A) Binding sites between miR-21 and SPRY1. Dual luciferase reporter assays were conducted to verify the combination.

(B and C) The mRNA and protein levels of SPRY1 in NT-2 cells.

(D) The CCK-8 assays were performed to determine the viability of NT-2 cells.

(E) Representative images and quantification of EDU assay.

(F) The autophagy flow in NT-2 cells was observed by confocal microscopy. Scale bar = 10 μm (confocal microscopy).

(G) The protein expressions of LC3 II/1 and beclin-1 and gray analysis normalized to GAPDH.

(H) Annexin V-FITC-PI analysis of cell apoptosis. Representative scatterplots and quantitative results were shown.

(I) Western blot analysis of cleaved caspase-3 and cleaved PARP expression and gray analysis normalized to GAPDH. Data are represented as mean ± SD; *$p < 0.05$; **$p < 0.01$; ***$p < 0.001$, ****$p < 0.0001$.

with 3-MA (a widely used autophagy inhibitor). The results showed that MEK162 significantly increased the percentage of early and late apoptotic cells (Figure 6F) and the expression of cleaved RARP and cleaved caspase-3 (Figure 6G). Remarkably, we found that 3-MA reversed apoptosis induced by MEK162 (Figures 6F and 6G). Therefore, we speculated that autophagy and apoptosis induced by inhibition of ERK phosphorylation were unsynchronized, and inhibition of autophagy leads to apoptosis decrease. Western blot demonstrated that MEK162 significantly promoted the expression of cleaved caspase-3 and cleaved PARP. Remarkably, MEK162-promoted apoptosis was significantly reversed by simultaneous MEG3 knockdown (Figure 6H). These results were further confirmed using flow cytometry assay (Figure 6I). Consequently, we considered that MEG3 promoted cell apoptosis by enhancing autophagy via the ERK signaling pathway.

NF-κB is an upstream transcription factor of MEG3

In this study, we incidentally detected that MEG3 expression was regulated by SPRY1 (Figure 7A). Bioinformatics prediction of PROMO, TFDB, and GTRD revealed that NF-κB was one of the transcription factors of MEG3, which revealed that NF-κB was one of the transcription factors of MEG3 (Figure 7B). Importantly, the phosphorylation level of NF-κB increased upon SPRY1 knockdown (Figure 7C). Consequently, we hypothesized a positive feedback loop between SPRY1/NF-κB and MEG3. Through sequence alignment using the JASPAR website (http://jaspar.genereg.net/analysis), we identified four potential NF-κB binding regions in the 2-kb stretch of the promoter region of MEG3 (Figure 7D). A chromatin immunoprecipitation (ChIP) assay was used to assess potential binding sites in the MEG3 promoter region. The results revealed that the 1708–1717 promoter region (#3 binding region) was most abundant among regions enriched by the p-NF-κB antibody (Figure 7E). As shown in Figure 7F, when the NF-κB binding sequence was mutated, the overexpression of luciferase expression was restored with the inhibition of NF-κB phosphorylation by phosphorylation inhibitor of NF-κB, IMD0354 (MCE, China), suggesting that this sequence was necessary for NF-κB to regulate MEG3 expression. Furthermore, our findings showed that inhibition of NF-κB phosphorylation promoted MEG3 expression (Figure 7G). Moreover, IMD0354 counteracted the SPRY1 knockdown effect on MEG3 expression, suggesting that NF-κB phosphorylation was intermediate between MEG3 and SPRY1 (Figure 7H).

DISCUSSION

Dysspermatogenesis is a multifaceted problem caused by meiotic and post-meiotic defects associated with impaired spermatogenesis.[46] The NOA is one of the most refractory male infertilities. Currently, the effects of clinical therapy are limited.[47] Even when mature spermatozoa are pathologically found in the testis of patients with NOA, the failure incidence of testicular sperm retrieval remains at 20%.[48] The NOA patients who experience treatment failure cannot obtain genetic offspring, which brings a heavy psychological burden to their families. Therefore, it is urgent to explore the pathogenesis of NOA and find potential therapeutic targets and effective therapeutic measures. Previous studies have identified numerous lncRNAs in humans and other mammals.[49] Notably, some lncRNAs connect with spermatogenesis.[50–52] However, studies on lncRNA expression patterns in spermatogenic dysfunction in patients with NOA remain limited.[53,54] Herein, lncRNA sequencing technologies were used to analyze lncRNA expression in the testes of patients with NOA. This study discovered that MEG3 expression was significantly upregulated in patients with NOA compared with that in normozoospermic individuals. Single-cell analysis revealed that MEG3 dominatingly expressed in germ cells. MEG3 is an imprinted gene located in the blot region of DLK1-MEG3 of chromosome 14q32.3. LncRNA MEG3 acts as an antitumor component and is involved in the pathophysiological processes of various human diseases.[55–58] Current studies lacked investigations pertaining to azoospermia. Herein, human NTERA-2 cells with spermatogonial stem cell characteristics were selected for cytological experiments *in vitro*. Subsequently, the role of MEG3 in spermatogenic cells was investigated.

LncRNAs can exert the "miRNA sponge" effect, therefore affecting the expression of downstream genes regulated by miRNAs, thus participating in various regulatory processes.[30,59–61] Although, miR-21 is a widely studied miRNA that has been verified to be associated with autophagy and apoptosis in human airway smooth muscle cells, hepatocellular carcinoma cells, and human vestibular schwannoma cells.[62–65] The correlation between MEG3 and miR-21 in NOA spermatogenesis remains to be determined. Our research found that dysregulation of MEG3 led to inactive proliferation and enhanced autophagy and apoptosis in NT-2 cells, and miR-21 separately exerted the reverse function of MEG3. Moreover, miR-21 mimics rescued inhibition of proliferation and promotion of autophagy and apoptosis induced by MEG3 overexpression. These results suggested that MEG3 functioned through competitive inhibition of miR-21. Our previous bioinformatics prediction found that SPRY1 was one of the downstream target genes of miR-21. Therefore, we speculated whether miR-21 regulated spermatogenesis in patients with NOA through SPRY1. We demonstrated that miR-21 inhibited translation of SPRY1. SPRY1 promoted autophagy and apoptosis and inhibited proliferation through the ERK/mTOR pathway in NT-2 cells. Western blotting analysis revealed that MEG3

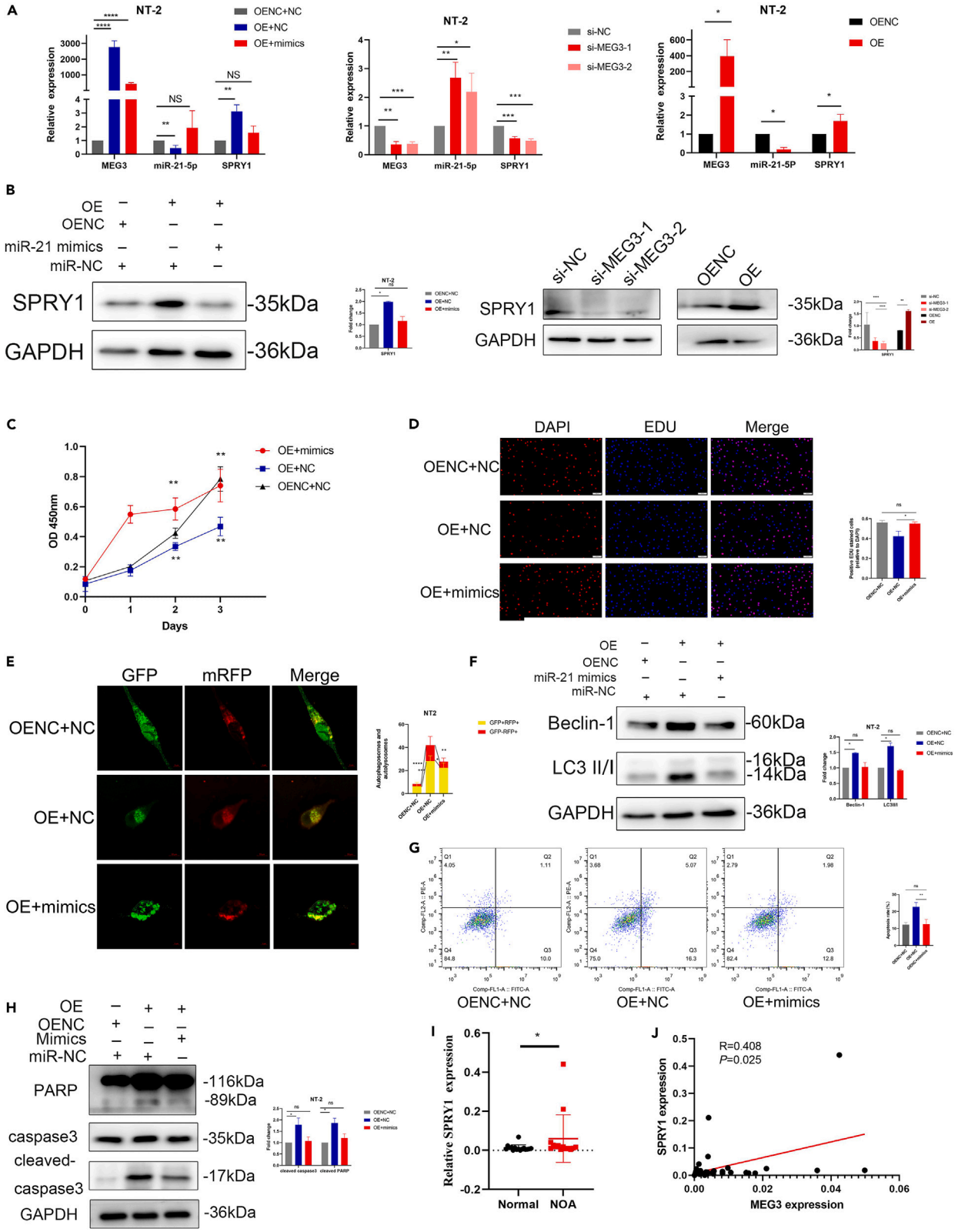
A
NT-2
OENC+NC
OE+NC
OE+mimics
Relative expression
MEG3
miR-21-5p
SPRY1
NS
si-NC
si-MEG3-1
si-MEG3-2
OENC
OE
B
OE
OENC
miR-21 mimics
miR-NC
SPRY1
GAPDH
-35kDa
-36kDa
C
OD 450nm
Days
D
DAPI
EDU
Merge
E
GFP
mRFP
Merge
F
Beclin-1
LC3 II/I
-60kDa
-16kDa
-14kDa
G
H
PARP
caspase3
cleaved-caspase3
-116kDa
-89kDa
-17kDa
I
Relative SPRY1 expression
Normal
NOA
J
R=0.408
P=0.025
SPRY1 expression
MEG3 expression

Figure 5. MEG3 promoted the miR-21 downstream SPRY1 by binding to miR-21

(A) Relative expression of miR-21, MEG3, and SPRY1 determined by RT-qPCR.

(B) Relative expression of SPRY1 determined by western blot.

(C) CCK-8 assays were performed to determine the viability of NT-2 cells.

(D) EDU assays were used to determine the cell viability of NT-2 cells.

(E) The autophagy flow in NT-2 cells was observed by confocal microscopy with indicated treatment. Scale bar = 5 μm (confocal microscopy).

(F) The co-effect of miR-21 mimics and MEG3 overexpression on the expression of LC3II and beclin-1 (right) and analysis normalized to GAPDH (left).

(G) Annexin V-FITC-PI analysis of cell apoptosis.

(H) Cleaved PARP and cleaved caspase-3 were detected by western blotting (left) and analysis normalized to GAPDH (right).

(I) SPRY1 expression in testicular tissues was detected by qPCR.

(J) Spearman's correlation analysis determined the relationship between MEG3 and SPRY1 expression in 30 clinical samples. Data are represented as mean ± SD; *$p < 0.05$; **$p < 0.01$; ***$p < 0.001$, ****$p < 0.0001$.

restrained ERK phosphorylation, whereas miR-21 mimics rescued this result. Considering the correlation between MEG3 and miR-21, we further considered that MEG3 acted as a ceRNA to competitively bind to miR-21, thereby blocking the translation inhibition of SPRY1.

Apoptosis is a crucial mechanism of programmed cell death in mammalian cells and has been considered as programmed cell death type I.[66] Consistent with apoptosis, autophagy has been considered a type II programmed cell death and is crucial in inducing cell death, eliminating toxic misfolded proteins and intracellular microorganisms, and promoting antigen presentation.[67,68] Crosstalk exists between the molecular mechanisms of autophagic and apoptotic under pathophysiological stimuli.[69] Mei Wang et al. detected that PI3K inhibitor 3-MA regulated apoptosis by inhibiting autophagy in Cd-treated testicular cells through the mTOR pathway in rats.[70] However, distinguishing whether both processes collaborate or occur independently is not easy. For example, a report showed that inhibition of the pro-apoptotic protease caspase 8 resulted in cell death and consequently enhanced autophagy. Conversely, knocking down of autophagy-related genes rescued the cell death.[71] Crighton et al. discovered that p53 induced cell death by activating autophagy through DRAM (damage-regulated autophagy modulator), a lysosomal protein.[72] Our study showed that MEK126 induced autophagy at 10 nM, and a higher concentration of MEK162 led to concurrent activation of autophagy and apoptosis. Therefore, we hypothesized that autophagy induced the caspase cascade of apoptosis. ERKs are the terminal kinases of MAPK signaling,[73] which regulate AMPK signaling in different layers under distinct circumstances.[74] Autophagy initiation is reciprocally regulated by mTORC1 and AMPK (protein kinase AMP-activated catalytic subunit alpha 1).[75] Therefore, we hypothesized that ERK phosphorylation coordinated the autophagic process with pro-apoptotic signals. Herein, we detected that MEK162 rescued 3-MA-inhibited autophagy, further promoting the apoptotic activity. Moreover, MEG3 knockdown rescued function of MEK162, demonstrating that the association between autophagy and apoptosis induced by MEG3 was consistent with the association induced by ERK phosphorylation.

Phosphorylated ERK1/2 (p-ERK1/2) can activate NF-κB, and phosphorylated NF-κB (p-NF-κB) transfers into the nucleus to bind to specific DNA fragments; inactive NF-κB is insulated in the cytoplasm by IκB family.[76] Herein, we used IMD-0354 to inhibit phosphorylation of NF-κB and found that IMD-0354 promoted MEG3 transcription. Additionally, IMD-0354 rescued the effect of SPRY1 knockdown on MEG3 expression. Zhang et al. proved that SPRY domain in the C-terminal region of SPRY1 physically interacted with ANK domain of NF-κB1.[77] Therefore, we considered SPRY1 could regulate MEG3 transcription by NF-κB. MEG3, as a ceRNA, regulated the expression of target gene transcripts by competing with miRNA reaction originals (MREs) for the same miRNA. SPRY1 possibly regulated MEG3 by a ceRNA mechanism. A positive feedback loop between MEG3 and SPRY1 presumably existed and presented that SPRY1 knockdown played a positive feedback role in MEG3 expression through the decrease of NF-κB phosphorylation.

MEG3 was first identified as the ortholog of gene trap locus 2 (Gtl2) in mice.[78] Takahashi et al. created Gtl2-mutant mice and found the deletion of Gtl2 and/or its DMR perhaps affected the expression of the neighboring imprinted genes via the cis-regulatory elements.[79] Our clinical data indicated that MEG3 is highly expressed in NOA patients. We introduced AAV9 overexpressing Gtl2 to mimic the high expression of MEG3 in testes in mice. Subsequently, the contribution of MEG3 to spermatogenesis through promoting autophagy and apoptosis and inhibiting proliferation of testicular spermatogenic cells was determined based on metrics including seminiferous tubule morphology and diameter, PCNA proliferation index, LC3 puncta, and TUNEL assay. Finally, we successfully identified MEG3 implication in testicular spermatogenic function, which aligns with previous *in vitro* findings.

Spermatogenesis consists of three stages: proliferation and differentiation of spermatogonia, maturation division of spermatocytes, and spermiogenesis (sperm formation).[80] Single-cell sequencing analysis showed that MEG3 was expressed in spermatogonia, spermatocytes, spermatids, and Sertoli cells in adult males with normal spermatogenesis in GSE106487. Analysis of single-cell sequencing from iNOA and normal adult samples in GSE149512 showed that MEG3 was highly expressed in NOA and significantly expressed differentially in spermatids and spermatogonia. We have proved the mechanism of MEG3-miR-21-SPRY1-NF-kB feedback loop in NT-2 cells. As for spermatids, we speculated overexpression of MEG3 might inhibit proliferation, promote autophagy and apoptosis, and further correlate to the number and structural changes of round spermatids during spermiogenesis stage. We also detected a small distribution of MEG3 in Sertoli cells. Sertoli cells provide the necessary support for the development of different germ cell types and create an adequate functional environment for germ cell development.[81] Sertoli cells that contribute to the changes of somatic microenvironment in NOA patients are manifest.[82] But the results of scRNA-seq and transcriptome analysis from Chen et al. did not identify any evidence supporting that changes in Sertoli cells lead to the loss of germ cells.[83] Therefore, the function of expression change of MEG3 in Sertoli cells on spermatogenesis remains to be verified.

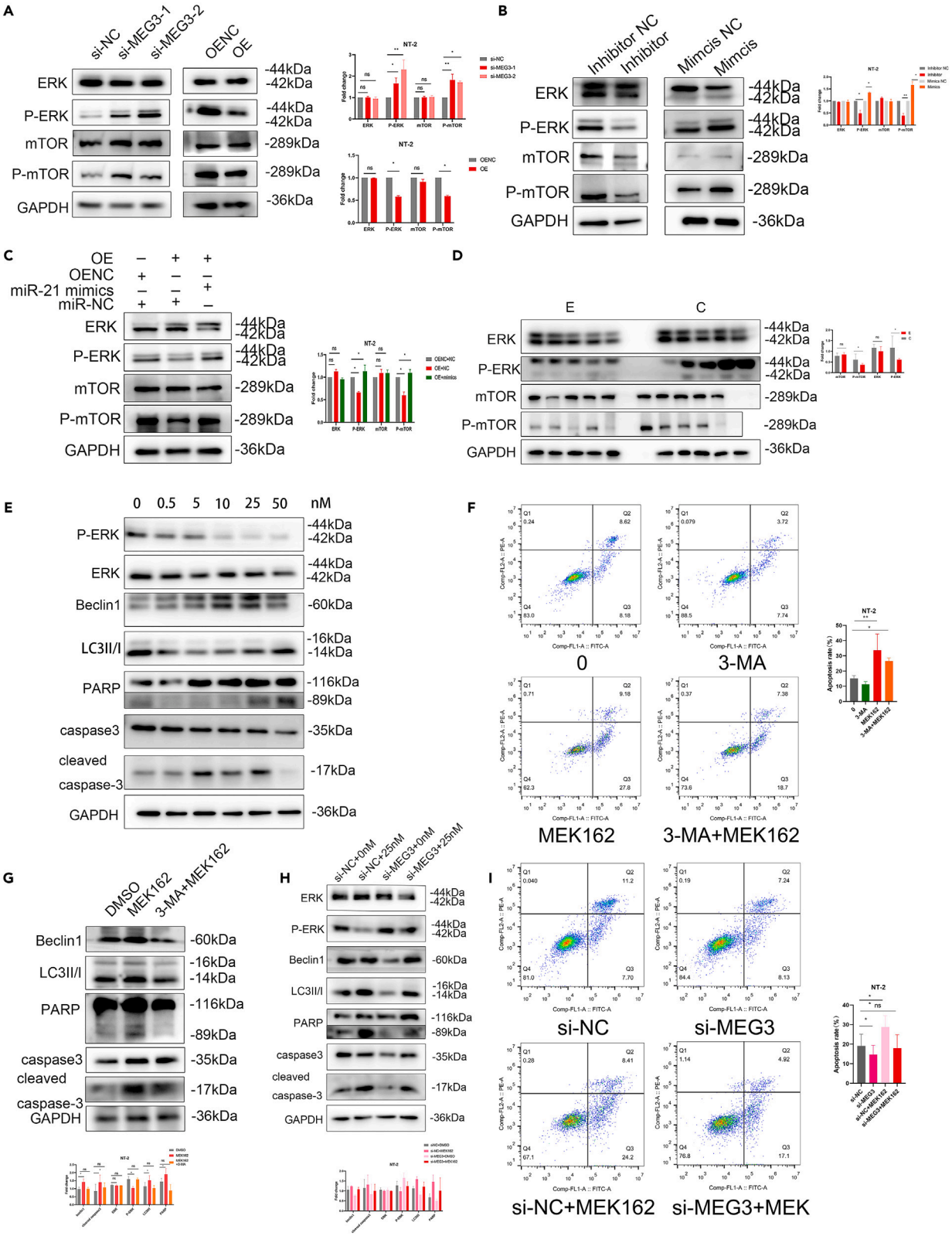
A
si-NC
si-MEG3-1
si-MEG3-2
OENC
OE
ERK
P-ERK
mTOR
P-mTOR
GAPDH
-44kDa
-42kDa
-289kDa
-36kDa
B
Inhibitor NC
Inhibitor
Mimcis NC
Mimcis
C
OE
OENC
miR-21 mimics
miR-NC
D
E
C
E
0 0.5 5 10 25 50 nM
Beclin1
LC3II/I
PARP
caspase3
cleaved
caspase-3
-60kDa
-16kDa
-14kDa
-116kDa
-89kDa
-35kDa
-17kDa
F
0
3-MA
MEK162
3-MA+MEK162
G
DMSO
MEK162
3-MA+MEK162
H
si-NC+0nM
si-NC+25nM
si-MEG3+0nM
si-MEG3+25nM
I
si-NC
si-MEG3
si-NC+MEK162
si-MEG3+MEK

Figure 6. MEG3 promoted apoptosis by enhancing the autophagy of spermatogenic cells through miR-21/SPRY1/ERK pathway

(A–C) ERK, P-ERK, mTOR, and P-mTOR were detected by western blot.

(D) Western blot images of mice testicular tissues.

(E) Western blot of NT-2 cells treated with a concentration gradient of MEK162.

(F) The effect of MEK162 with or without 3-MA on apoptosis of NT-2 cells was detected using Annexin V-FITC-PI kit.

(G) Cleaved PARP and cleaved caspase-3 were detected using western blot with the MEK162 and 3-MA treatment, analysis normalized to GAPDH.

(H) Rescue assay detected by western blot.

(I) Rescue assay detected by Annexin V-FITC-PI kit. Data are represented as mean ± SD; *$p < 0.05$; **$p < 0.01$; ***$p < 0.001$, ****$p < 0.0001$.

Conclusion

Our results demonstrate that the lncRNA MEG3/miR-21/SPRY1 axis may act as ceRNA regulatory network and regulate spermatogenic cell proliferation, autophagy, and apoptosis, resulting in spermatogenesis disability. Our findings provided insights into MEG3 and theoretical basis for the development of gene therapy drugs targeting MEG3 in testis for non-obstructive azoospermia in the future.

Limitations of the study

The function of expression change of MEG3 in Sertoli cells on spermatogenesis remains to be verified, which will be the direction of our future research.

RESOURCES AVAILABILITY

Lead contact

Further information and requests for resources and reagents should be directed to and will be fulfilled by the Lead Contact, Wenyan Song (csxokgzr@sina.com).

Materials availability

The plasmids generated in this study can be requested from the lead contact, Wenyan Song (csxokgzr@sina.com).

Data and code availability

- The RNA-seq data generated for this study have been deposited at the Gene Expression Omnibus (GSE241326) under the accession code. Clinical information data have been deposited at Mendeley Data, V1, https://doi.org/10.17632/bwzt7b9tr3.1. They are publicly available as of the date of publication. RT-qPCR data reported in this paper will be shared by the lead contact upon reasonable request.
- This paper does not report original code.
- Any additional information required to reanalyze the data reported in this paper is available from the lead contact upon request.

ACKNOWLEDGMENTS

This work was supported by National Natural Science Foundation of China (8187061015).

AUTHOR CONTRIBUTIONS

X.F., X.L., and Y.M. made equal contributions to this research. W.Y.S. and X.Y.F. designed the experiments; X.Y.F. conducted the experiments; X.Y.F. and X.T.L. performed the mechanism experiments and analyzed the data. Y.J.M. contributed to the clinical sample collection; H.R.G. participated in the animal study; N.S. and M.J.S. analyzed the clinical data. X.Y.F. drafted the manuscript. W.Y.S., G.D.Y., and H.X.J. revised the manuscript. All authors read and approved the final manuscript.

DECLARATION OF INTERESTS

The authors declare no conflict of interest.

STAR★METHODS

Detailed methods are provided in the online version of this paper and include the following:

- KEY RESOURCES TABLE
- EXPERIMENTAL MODEL AND STUDY PARTICIPANTS
  - Testicular tissues
  - Microinjection of virus particles
- METHOD DETAILS
  - RNA purification, RNA-Seq library construction and sequencing
  - Cell lines and cell culture
  - Plasmid construction and cell transfection
  - Reverse transcription and quantitative real-time PCR (qPCR)
  - Western blot
  - Immunohistochemical (IHC) staining

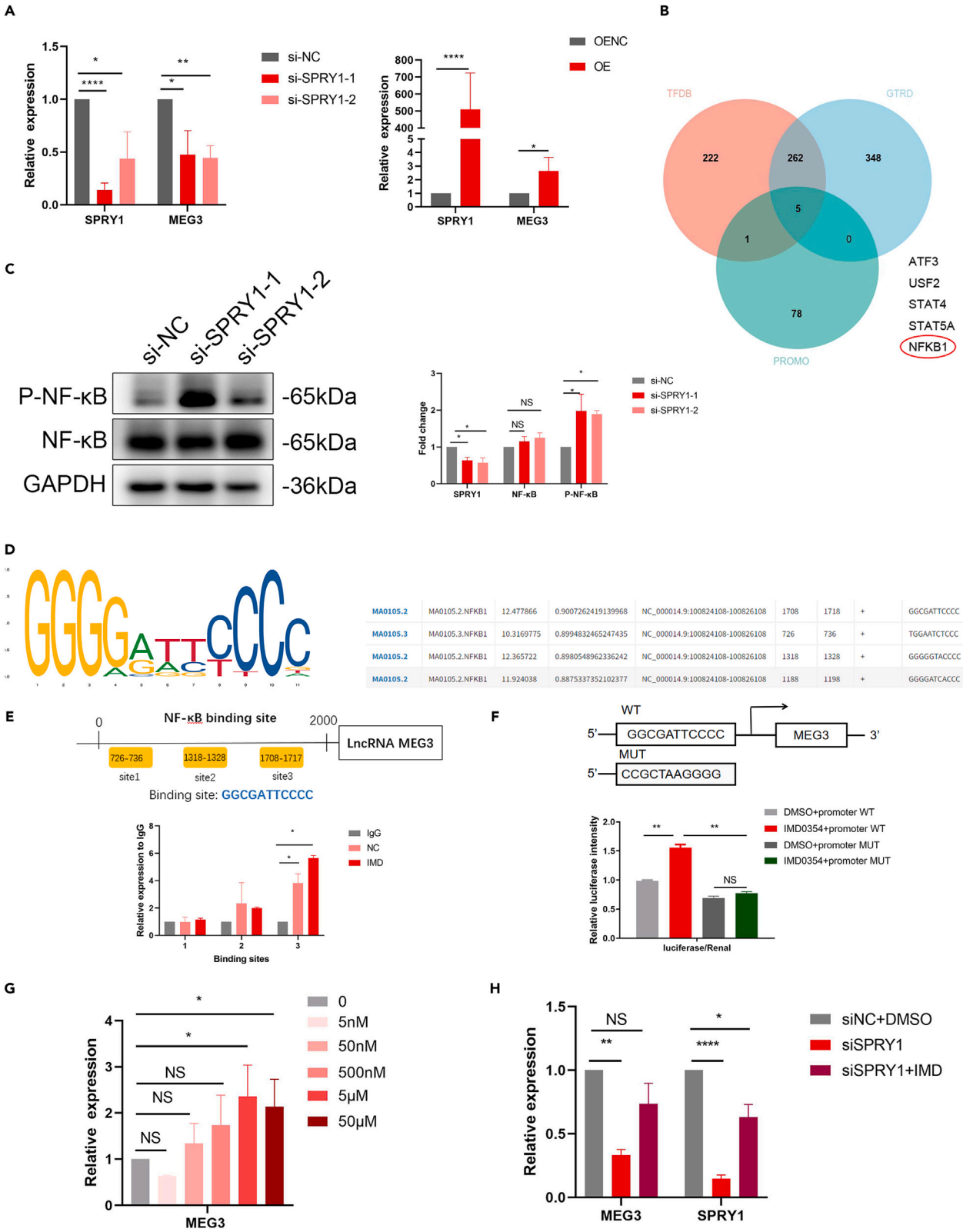
A
Relative expression
si-NC
si-SPRY1-1
si-SPRY1-2
SPRY1
MEG3
OENC
OE
B
TFDB
GTRD
PROMO
222
262
348
5
1
0
78
ATF3
USF2
STAT4
STAT5A
NFKB1
C
si-NC
si-SPRY1-1
si-SPRY1-2
P-NF-κB
NF-κB
GAPDH
-65kDa
-65kDa
-36kDa
Fold change
NS
SPRY1
NF-κB
P-NF-κB
D
MA0105.2 MA0105.2.NFKB1 12.477866 0.9007262419139968 NC_000014.9:100824108-100826108 1708 1718 + GGCGATTCCCC
MA0105.3 MA0105.3.NFKB1 10.3169775 0.8994832465247435 NC_000014.9:100824108-100826108 726 736 + TGGAATCTCCC
MA0105.2 MA0105.2.NFKB1 12.365722 0.8980548962336242 NC_000014.9:100824108-100826108 1318 1328 + GGGGGTACCCC
MA0105.2 MA0105.2.NFKB1 11.924038 0.8875337352102377 NC_000014.9:100824108-100826108 1188 1198 + GGGGATCACCC
E
NF-κB binding site
0
2000
LncRNA MEG3
726-736
1318-1328
1708-1717
site1
site2
site3
Binding site: GGCGATTCCCC
Relative expression to IgG
IgG
NC
IMD
Binding sites
F
WT
5'
GGCGATTCCCC
MEG3
3'
MUT
5'
CCGCTAAGGGG
DMSO+promoter WT
IMD0354+promoter WT
DMSO+promoter MUT
IMD0354+promoter MUT
Relative luciferase intensity
NS
luciferase/Renal
G
Relative expression
NS
0
5nM
50nM
500nM
5μM
50μM
MEG3
H
Relative expression
NS
siNC+DMSO
siSPRY1
siSPRY1+IMD
MEG3
SPRY1

Figure 7. NF-κB is an upstream transcription factor (TF) of MEG3

(A) RT-qPCR illustrated the effect of SPRY1 on MEG3 expression.

(B) Bioinformatic prediction from the PROMO, TFDB, and GTRD databases.

(C) Western blot demonstrated SPRY1 regulated the phosphorylation of NF-κB.

(D) NF-κB binding sequence in the MEG3 promoter region predicted by the JASPAR website.

(E) ChIP assay of NT-2 cells using an antibody against p-NF-κB.

(F) Dual-luciferase reporter assay showed that the predictive binding site is necessary for the for the Luc expression with the inhibition of p-NF-κB.

(G) Relative levels of MEG3 in NT-2 cells treated with an inhibitor of NF-κB phosphorylation, IMD-0354.

(H) Relative levels of MEG3 in NT-2 cells treated with IMD-0354 with or without SPRY1 siRNA transfection. Data are represented as mean ± SD; *$p < 0.05$; **$p < 0.01$; ***$p < 0.001$, ****$p < 0.0001$.

- Heamatoxylin and eosin
- FISH
- Bioinformatic prediction
- RNA immunoprecipitation assay
- RNA pull-down assay
- Cell counting kit-8 assay
- EDU assay
- Flow cytometry
- TUNEL
- ChIP assay
- Dual luciferase reporter assay
- Immunostaining
- GFP-mRFP-LC3 lentivirus transfection and confocal microscopy

● QUANTIFICATION AND STATISTICAL ANALYSIS

SUPPLEMENTAL INFORMATION

Supplemental information can be found online at https://doi.org/10.1016/j.isci.2024.110904.

Received: October 25, 2023
Revised: April 20, 2024
Accepted: September 5, 2024
Published: September 10, 2024

REFERENCES

1. Cocuzza, M., Alvarenga, C., and Pagani, R. (2013). The epidemiology and etiology of azoospermia. Clinics *68*, 15–26. https://doi.org/10.6061/clinics/2013(sup01)03.
2. Olesen, I.A., Andersson, A.M., Aksglaede, L., Skakkebaek, N.E., Rajpert-de Meyts, E., Joergensen, N., and Juul, A. (2017). Clinical, genetic, biochemical, and testicular biopsy findings among 1,213 men evaluated for infertility. Fertil. Steril. *107*, 74–82.e7. https://doi.org/10.1016/j.fertnstert.2016.09.015.
3. Maduro, M.R., and Lamb, D.J. (2002). Understanding new genetics of male infertility. J. Urol. *168*, 2197–2205. https://doi.org/10.1097/07.ju.0000023290.61978.b2.
4. Agarwal, A., Majzoub, A., Parekh, N., and Henkel, R. (2020). A Schematic Overview of the Current Status of Male Infertility Practice. World J. Mens Health *38*, 308–322. https://doi.org/10.5534/wjmh.190068.
5. Wosnitzer, M., Goldstein, M., and Hardy, M.P. (2014). Review of Azoospermia. Spermatogenesis *4*, e28218. https://doi.org/10.4161/spmg.28218.
6. Practice Committee of American Society for Reproductive Medicine in collaboration with Society for Male Reproduction and Urology (2008). Reproductive Medicine in collaboration with Society for Male, R. & Urology. The management of infertility due to obstructive azoospermia. Fertil. Steril. *90*, S121–S124. https://doi.org/10.1016/j.fertnstert.2008.08.096.
7. Jarow, J.P., Espeland, M.A., and Lipshultz, L.I. (1989). Evaluation of the azoospermic patient. J. Urol. *142*, 62–65. https://doi.org/10.1016/s0022-5347(17)38662-7.
8. Jarvi, K., Lo, K., Grober, E., Mak, V., Fischer, A., Grantmyre, J., Zini, A., Chan, P., Patry, G., Chow, V., and Domes, T. (2015). The workup and management of azoospermic males. Canadian Urological Association Journal *9*, 229–235. https://doi.org/10.5489/cuaj.3209.
9. Tournaye, H., Camus, M., Vandervorst, M., Nagy, Z., Joris, H., Van Steirteghem, A., and Devroey, P. (1997). Surgical sperm retrieval for intracytoplasmic sperm injection. Int. J. Androl. *20*, 69–73.
10. Visser, L., and Repping, S. (2010). Unravelling the genetics of spermatogenic failure. Reproduction *139*, 303–307. https://doi.org/10.1530/rep-09-0229.
11. Kotaja, N. (2014). MicroRNAs and spermatogenesis. Fertil. Steril. *101*, 1552–1562. https://doi.org/10.1016/j.fertnstert.2014.04.025.
12. Cioppi, F., Rosta, V., and Krausz, C. (2021). Genetics of Azoospermia. Int. J. Mol. Sci. *22*, 3264. https://doi.org/10.3390/ijms22063264.
13. Shen, Y., Wu, X., Li, Q., Huang, X., Wang, J., Zhao, L., Zhang, T., and Xuan, X. (2022). Identification and Potential Value of Candidate Genes in Patients With Non-obstructive Azoospermia. Urology *164*, 133–139. https://doi.org/10.1016/j.urology.2022.02.009.
14. Robles, V., Valcarce, D.G., and Riesco, M.F. (2019). Non-coding RNA regulation in reproduction: Their potential use as biomarkers. Noncoding. RNA Res. *4*, 54–62. https://doi.org/10.1016/j.ncrna.2019.04.001.
15. Daneshmandpour, Y., Bahmanpour, Z., Hamzeiy, H., Mazaheri Moghaddam, M., Mazaheri Moghaddam, M., Khademi, B., and Sakhinia, E. (2020). MicroRNAs association with azoospermia, oligospermia, asthenozoospermia, and teratozoospermia: a systematic review. J. Assist. Reprod. Genet. *37*, 763–775. https://doi.org/10.1007/s10815-019-01674-9.
16. Mercer, T.R., Dinger, M.E., and Mattick, J.S. (2009). Long non-coding RNAs: insights into functions. Nat. Rev. Genet. *10*, 155–159. https://doi.org/10.1038/nrg2521.
17. Willingham, A.T., Orth, A.P., Batalov, S., Peters, E.C., Wen, B.G., Aza-Blanc, P., Hogenesch, J.B., and Schultz, P.G. (2005). A strategy for probing the function of noncoding RNAs finds a repressor of NFAT. Science (New York, N.Y.) *309*, 1570–1573. https://doi.org/10.1126/science.1115901.
18. Carrieri, C., Cimatti, L., Biagioli, M., Beugnet, A., Zucchelli, S., Fedele, S., Pesce, E., Ferrer, I., Collavin, L., Santoro, C., et al. (2012). Long non-coding antisense RNA controls Uchl1 translation through an embedded SINEB2 repeat. Nature *491*, 454–457. https://doi.org/10.1038/nature11508.
19. Liu, K., Mao, X., Chen, Y., Li, T., and Ton, H. (2018). Regulatory role of long non-coding RNAs during reproductive disease. Am. J. Transl. Res. *10*, 1–12.
20. Prasanth, K.V., Prasanth, S.G., Xuan, Z., Hearn, S., Freier, S.M., Bennett, C.F., Zhang,

M.Q., and Spector, D.L. (2005). Regulating gene expression through RNA nuclear retention. Cell *123*, 249–263. https://doi.org/10.1016/j.cell.2005.08.033.

21. Joshi, M., and Rajender, S. (2020). Long non-coding RNAs (lncRNAs) in spermatogenesis and male infertility. Reprod. Biol. Endocrinol. *18*, 103. https://doi.org/10.1186/s12958-020-00660-6.
22. Rolland, A.D., Evrard, B., Darde, T.A., Le Béguec, C., Le Bras, Y., Bensalah, K., Lavoué, S., Jost, B., Primig, M., Dejucq-Rainsford, N., et al. (2019). RNA profiling of human testicular cells identifies syntenic lncRNAs associated with spermatogenesis. Hum. Reprod. *34*, 1278–1290. https://doi.org/10.1093/humrep/dez063.
23. Lü, M., Tian, H., Cao, Y.X., He, X., Chen, L., Song, X., Ping, P., Huang, H., and Sun, F. (2015). Downregulation of miR-320a/383-sponge-like long non-coding RNA NLC1-C (narcolepsy candidate-region 1 genes) is associated with male infertility and promotes testicular embryonal carcinoma cell proliferation. Cell Death Dis. *6*, e1960. https://doi.org/10.1038/cddis.2015.267.
24. Arafat, M., Har-Vardi, I., Harlev, A., Levitas, E., Zeadna, A., Abofoul-Azab, M., Dyomin, V., Sheffield, V.C., Lunenfeld, E., Huleihel, M., and Parvari, R. (2017). Mutation in TDRD9 causes non-obstructive azoospermia in infertile men. J. Med. Genet. *54*, 633–639. https://doi.org/10.1136/jmedgenet-2017-104514.
25. Riera-Escamilla, A., Enguita-Marruedo, A., Moreno-Mendoza, D., Chianese, C., Sleddens-Linkels, E., Contini, E., Benelli, M., Natali, A., Colpi, G.M., Ruiz-Castañé, E., et al. (2019). Sequencing of a 'mouse azoospermia' gene panel in azoospermic men: identification of RNF212 and STAG3 mutations as novel genetic causes of meiotic arrest. Hum. Reprod. *34*, 978–988. https://doi.org/10.1093/humrep/dez042.
26. Frankel, L.B., Lubas, M., and Lund, A.H. (2017). Emerging connections between RNA and autophagy. Autophagy *13*, 3–23. https://doi.org/10.1080/15548627.2016.1222992.
27. Zhang, J., Zhang, P., Wang, L., Piao, H.L., and Ma, L. (2014). Long non-coding RNA HOTAIR in carcinogenesis and metastasis. Acta Biochim. Biophys. Sin. *46*, 1–5. https://doi.org/10.1093/abbs/gmt117.
28. Yang, L., Zhang, X., Li, H., and Liu, J. (2016). The long noncoding RNA HOTAIR activates autophagy by upregulating ATG3 and ATG7 in hepatocellular carcinoma. Mol. Biosyst. *12*, 2605–2612. https://doi.org/10.1039/c6mb00114a.
29. Chen, J., Yu, Y., Li, H., Hu, Q., Chen, X., He, Y., Xue, C., Ren, F., Ren, Z., Li, J., et al. (2019). Long non-coding RNA PVT1 promotes tumor progression by regulating the miR-143/HK2 axis in gallbladder cancer. Mol. Cancer *18*, 33. https://doi.org/10.1186/s12943-019-0947-9.
30. Kong, X., Duan, Y., Sang, Y., Li, Y., Zhang, H., Liang, Y., Liu, Y., Zhang, N., and Yang, Q. (2019). LncRNA-CDC6 promotes breast cancer progression and function as ceRNA to target CDC6 by sponging microRNA-215. J. Cell. Physiol. *234*, 9105–9117. https://doi.org/10.1002/jcp.27587.
31. Wu, W., Hu, Z., Qin, Y., Dong, J., Dai, J., Lu, C., Zhang, W., Shen, H., Xia, Y., and Wang, X. (2012). Seminal plasma microRNAs: potential biomarkers for spermatogenesis status. Mol. Hum. Reprod. *18*, 489–497. https://doi.org/10.1093/molehr/gas022.
32. Wang, L., and Xu, C. (2015). Role of microRNAs in mammalian spermatogenesis and testicular germ cell tumors. Reproduction *149*, R127–R137. https://doi.org/10.1530/rep-14-0239.
33. Bartel, D.P. (2004). MicroRNAs: genomics, biogenesis, mechanism, and function. Cell *116*, 281–297. https://doi.org/10.1016/s0092-8674(04)00045-5.
34. Li, K., Gong, Q., Xiang, X.D., Guo, G., Liu, J., Zhao, L., Li, J., Chen, N., Li, H., Zhang, L.J., et al. (2023). HNRNPA2B1-mediated m(6)A modification of lncRNA MEG3 facilitates tumorigenesis and metastasis of non-small cell lung cancer by regulating miR-21-5p/PTEN axis. J. Transl. Med. *21*, 382. https://doi.org/10.1186/s12967-023-04190-8.
35. Yang, S., Feng, L., Zhang, Q., Wu, L., Zhao, Q., Hou, Y., Yan, B., and Zhang, S. (2023). Overexpression of lncRNA-MEG3 inhibits endometrial cell proliferation and invasion via miR-21-5p/DNMT3B/Twist. Clinics *78*, 100235. https://doi.org/10.1016/j.clinsp.2023.100235.
36. Wu, L., Zhu, L., Li, Y., Zheng, Z., Lin, X., and Yang, C. (2020). LncRNA MEG3 promotes melanoma growth, metastasis and formation through modulating miR-21/E-cadherin axis. Cancer Cell Int. *20*, 12. https://doi.org/10.1186/s12935-019-1087-4.
37. Erdem, M.G., Unlu, O., and Demirci, M. (2023). Could Long Non-Coding RNA MEG3 and PTENP1 Interact with miR-21 in the Pathogenesis of Non-Alcoholic Fatty Liver Disease? Biomedicines *11*, 574. https://doi.org/10.3390/biomedicines11020574.
38. Liu, H., Cai, X., Liu, J., Zhang, F., He, A., and Li, R. (2021). The MEG3 lncRNA promotes trophoblastic cell growth and invasiveness in preeclampsia by acting as a sponge for miR-21, which regulates BMPR2 levels. Eur. J. Histochem. *65*, 3323. https://doi.org/10.4081/ejh.2021.3323.
39. Wang, Y., Guo, Q., Zhao, Y., Chen, J., Wang, S., Hu, J., and Sun, Y. (2014). BRAF-activated long non-coding RNA contributes to cell proliferation and activates autophagy in papillary thyroid carcinoma. Oncol. Lett. *8*, 1947–1952. https://doi.org/10.3892/ol.2014.2487.
40. Darimipourain, M., Wang, S., Ittmann, M., and Kwabi-Addo, B. (2011). Transcriptional and post-transcriptional regulation of Sprouty1, a receptor tyrosine kinase inhibitor in prostate cancer. Prostate Cancer Prostatic Dis. *14*, 279–285. https://doi.org/10.1038/pcan.2011.33.
41. Masoumi-Moghaddam, S., Amini, A., Ehteda, A., Wei, A.Q., and Morris, D.L. (2014). The expression of the Sprouty 1 protein inversely correlates with growth, proliferation, migration and invasion of ovarian cancer cells. J. Ovarian Res. *7*, 61. https://doi.org/10.1186/1757-2215-7-61.
42. Lee, S., Bui Nguyen, T.M., Kovalenko, D., Adhikari, N., Grindle, S., Polster, S.P., Friesel, R., Ramakrishnan, S., and Hall, J.L. (2010). Sprouty1 inhibits angiogenesis in association with up-regulation of p21 and p27. Mol. Cell. Biochem. *338*, 255–261. https://doi.org/10.1007/s11010-009-0359-z.
43. Liu, E., Lv, L., Zhan, Y., Ma, Y., Feng, J., He, Y., Wen, Y., Zhang, Y., Pu, Q., Ji, F., et al. (2021). METTL3/N6-methyladenosine/miR-21-5p promotes obstructive renal fibrosis by regulating inflammation through SPRY1/ERK/NF-κB pathway activation. J. Cell Mol. Med. *25*, 7660–7674. https://doi.org/10.1111/jcmm.16603.
44. Li, N., Wang, Z., Gao, F., Lei, Y., and Li, Z. (2020). Melatonin ameliorates renal fibroblast-myofibroblast transdifferentiation and renal fibrosis through miR-21-5p regulation. J. Cell Mol. Med. *24*, 5615–5628. https://doi.org/10.1111/jcmm.15221.
45. Pu, M., Chen, J., Tao, Z., Miao, L., Qi, X., Wang, Y., and Ren, J. (2019). Regulatory network of miRNA on its target: coordination between transcriptional and post-transcriptional regulation of gene expression. Cell. Mol. Life Sci. *76*, 441–451. https://doi.org/10.1007/s00018-018-2940-7.
46. Steger, K., Aleithe, I., Behre, H., and Bergmann, M. (1998). The proliferation of spermatogonia in normal and pathological human seminiferous epithelium: an immunohistochemical study using monoclonal antibodies against Ki-67 protein and proliferating cell nuclear antigen. Mol. Hum. Reprod. *4*, 227–233. https://doi.org/10.1093/molehr/4.3.227.
47. Vij, S.C., Sabanegh, E., Jr., and Agarwal, A. (2018). Biological therapy for non-obstructive azoospermia. Expet Opin. Biol. Ther. *18*, 19–23. https://doi.org/10.1080/14712598.2018.1380622.
48. Achermann, A.P.P., Pereira, T.A., and Esteves, S.C. (2021). Microdissection testicular sperm extraction (micro-TESE) in men with infertility due to nonobstructive azoospermia: summary of current literature. Int. Urol. Nephrol. *53*, 2193–2210. https://doi.org/10.1007/s11255-021-02979-4.
49. Sarropoulos, I., Marin, R., Cardoso-Moreira, M., and Kaessmann, H. (2019). Developmental dynamics of lncRNAs across mammalian organs and species. Nature *571*, 510–514. https://doi.org/10.1038/s41586-019-1341-x.
50. Sun, T.C., Zhang, Y., Yu, K., Li, Y., Yu, H., Zhou, S.J., Wang, Y.P., Deng, S.L., and Tian, L. (2021). LncRNAs induce oxidative stress and spermatogenesis by regulating endoplasmic reticulum genes and pathways. Aging (Albany NY) *13*, 13764–13787. https://doi.org/10.18632/aging.202971.
51. Hu, K., Gao, Y., Xu, Y., He, C., Wang, K., Li, L., Liao, Y., Liu, X., and Liang, M. (2022). Overexpression of lncRNA-Gm2044 in spermatogonia impairs spermatogenesis in partial seminiferous tubules. Poultry Sci. *101*, 101930. https://doi.org/10.1016/j.psj.2022.101930.
52. Hu, K., Li, L., Liao, Y., and Liang, M. (2018). LncRNA Gm2044 highly expresses in spermatocyte and inhibits Utf1 translation by interacting with Utf1 mRNA. Genes Genomics *40*, 781–787. https://doi.org/10.1007/s13258-018-0690-4.
53. Hua, R., Chu, Q., Guo, F., Chen, Q., Li, M., Zhou, X., and Zhu, Y. (2023). DNM3OS Enhances the Apoptosis and Senescence of Spermatogonia Associated with Nonobstructive Azoospermia by Providing miR-214-5p and Decreasing E2F2 Expression. Anal. Cell Pathol. *2023*, 1477658. https://doi.org/10.1155/2023/1477658.
54. Zhou, F., Chen, W., Cui, Y., Liu, B., Yuan, Q., Li, Z., and He, Z. (2020). miRNA-122-5p stimulates the proliferation and DNA synthesis and inhibits the early apoptosis of human spermatogonial stem cells by targeting CBL and competing with lncRNA CASC7. Aging (Albany NY) *12*, 25528–25546. https://doi.org/10.18632/aging.104158.
55. Al-Rugeebah, A., Alanazi, M., and Parine, N.R. (2019). MEG3: an Oncogenic Long Non-coding RNA in Different Cancers. Pathol.

Oncol. Res. *25*, 859–874. https://doi.org/10.1007/s12253-019-00614-3.
56. Li, X., Bai, C., Wang, H., Wan, T., and Li, Y. (2022). LncRNA MEG3 regulates autophagy and pyroptosis via FOXO1 in pancreatic β-cells. Cell. Signal. *92*, 110247. https://doi.org/10.1016/j.cellsig.2022.110247.
57. Zhou, W., Wang, Z., Tao, Y., Chen, C., Zhang, Q., Liu, Z., Li, L., Xia, P., and Ye, Z. (2022). LncRNA-MEG3 attenuates hyperglycemia-induced damage by enhancing mitochondrial translocation of HSP90A in the primary hippocampal neurons. Exp. Cell Res. *419*, 113320. https://doi.org/10.1016/j.yexcr.2022.113320.
58. Meng, J., Ding, T., Chen, Y., Long, T., Xu, Q., Lian, W., and Liu, W. (2021). LncRNA-Meg3 promotes Nlrp3-mediated microglial inflammation by targeting miR-7a-5p. Int. Immunopharm. *90*, 107141. https://doi.org/10.1016/j.intimp.2020.107141.
59. Lewandowski, J.P., Dumbović, G., Watson, A.R., Hwang, T., Jacobs-Palmer, E., Chang, N., Much, C., Turner, K.M., Kirby, C., Rubinstein, N.D., et al. (2020). The Tug1 lncRNA locus is essential for male fertility. Genome Biol. *21*, 237. https://doi.org/10.1186/s13059-020-02081-5.
60. Braga, E.A., Fridman, M.V., Moscovtsev, A.A., Filippova, E.A., Dmitriev, A.A., and Kushlinskii, N.E. (2020). LncRNAs in Ovarian Cancer Progression, Metastasis, and Main Pathways: ceRNA and Alternative Mechanisms. Int. J. Mol. Sci. *21*, 8855. https://doi.org/10.3390/ijms21228855.
61. Wang, J., Huang, J., Guo, Y., Fu, Y., Cao, Y., Zhou, K., Ma, J., Lv, B., and Huang, W. (2022). Identification and functional analysis of LncRNA-XIST ceRNA network in prostate cancer. BMC Cancer *22*, 935. https://doi.org/10.1186/s12885-022-10007-6.
62. Sun, P., Zhang, S., Wu, D., Qian, Y., Xiao, X., and Zhang, Q. (2022). MiR-21 modulates proliferation and apoptosis of human airway smooth muscle cells by regulating autophagy via PARP-1/AMPK/mTOR signalling pathway. Respir. Physiol. Neurobiol. *301*, 103891. https://doi.org/10.1016/j.resp.2022.103891.
63. Yang, P., Sun, D., and Jiang, F. (2018). Ailanthone Promotes Human Vestibular Schwannoma Cell Apoptosis and Autophagy by Downregulation of miR-21. Oncol. Res. *26*, 941–948. https://doi.org/10.3727/096504018x15149775533331.
64. Li, W., Dong, X., He, C., Tan, G., Li, Z., Zhai, B., Feng, J., Jiang, X., Liu, C., Jiang, H., and Sun, X. (2019). LncRNA SNHG1 contributes to sorafenib resistance by activating the Akt pathway and is positively regulated by miR-21 in hepatocellular carcinoma cells. J. Exp. Clin. Cancer Res. *38*, 183. https://doi.org/10.1186/s13046-019-1177-0.
65. Taheri, M., Safarzadeh, A., Hussen, B.M., Ghafouri-Fard, S., and Baniahmad, A. (2022). LncRNA/miRNA/mRNA Network Introduces Novel Biomarkers in Prostate Cancer. Cells *11*, 3776. https://doi.org/10.3390/cells11233776.
66. Rosenfeldt, M.T., and Ryan, K.M. (2009). The role of autophagy in tumour development and cancer therapy. Expet Rev. Mol. Med. *11*, e36. https://doi.org/10.1017/s1462399409001306.
67. Hotchkiss, R.S., Strasser, A., McDunn, J.E., and Swanson, P.E. (2009). Cell death. N. Engl. J. Med. *361*, 1570–1583. https://doi.org/10.1056/NEJMra0901217.
68. Li, X., He, S., and Ma, B. (2020). Autophagy and autophagy-related proteins in cancer. Mol. Cancer *19*, 12. https://doi.org/10.1186/s12943-020-1138-4.
69. Zhang, N., Ji, N., Jiang, W.M., Li, Z.Y., Wang, M., Wen, J.M., Li, Y., Chen, X., and Chen, J.M. (2015). Hypoxia-induced autophagy promotes human prostate stromal cells survival and ER-stress. Biochem. Biophys. Res. Commun. *464*, 1107–1112. https://doi.org/10.1016/j.bbrc.2015.07.086.
70. Wang, M., Wang, X.F., Li, Y.M., Chen, N., Fan, Y., Huang, W.K., Hu, S.F., Rao, M., Zhang, Y.Z., and Su, P. (2020). Cross-talk between autophagy and apoptosis regulates testicular injury/recovery induced by cadmium via PI3K with mTOR-independent pathway. Cell Death Dis. *11*, 46. https://doi.org/10.1038/s41419-020-2246-1.
71. Yu, L., Alva, A., Su, H., Dutt, P., Freundt, E., Welsh, S., Baehrecke, E.H., and Lenardo, M.J. (2004). Regulation of an ATG7-beclin 1 program of autophagic cell death by caspase-8. Science (New York, N.Y.) *304*, 1500–1502. https://doi.org/10.1126/science.1096645.
72. Crighton, D., Wilkinson, S., O'Prey, J., Syed, N., Smith, P., Harrison, P.R., Gasco, M., Garrone, O., Crook, T., and Ryan, K.M. (2006). DRAM, a p53-induced modulator of autophagy, is critical for apoptosis. Cell *126*, 121–134. https://doi.org/10.1016/j.cell.2006.05.034.
73. Yuan, J., Dong, X., Yap, J., and Hu, J. (2020). The MAPK and AMPK signalings: interplay and implication in targeted cancer therapy. J. Hematol. Oncol. *13*, 113. https://doi.org/10.1186/s13045-020-00949-4.
74. Li, Y., Xia, J., Jiang, N., Xian, Y., Ju, H., Wei, Y., and Zhang, X. (2018). Corin protects H(2)O(2)-induced apoptosis through PI3K/AKT and NF-κB pathway in cardiomyocytes. Biomed. Pharmacother. *97*, 594–599. https://doi.org/10.1016/j.biopha.2017.10.090.
75. Kim, Y.C., and Guan, K.L. (2015). mTOR: a pharmacologic target for autophagy regulation. J. Clin. Invest. *125*, 25–32. https://doi.org/10.1172/jci73939.
76. White, S., Lin, L., and Hu, K. (2020). NF-κB and tPA Signaling in Kidney and Other Diseases. Cells *9*, 1348. https://doi.org/10.3390/cells9061348.
77. Zhang, M.F., Wan, S.C., Chen, W.B., Yang, D.H., Liu, W.Q., Li, B.L., Aierken, A., Du, X.M., Li, Y.X., Wu, W.P., et al. (2023). Transcription factor Dmrt1 triggers the SPRY1-NF-kappa pathway to maintain testicular immune homeostasis and male fertility. Zool. Res. *44*, 505–521. https://doi.org/10.24272/j.issn.2095-8137.2022.440.
78. Schuster-Gossler, K., Bilinski, P., Sado, T., Ferguson-Smith, A., and Gossler, A. (1998). The mouse Gtl2 gene is differentially expressed during embryonic development, encodes multiple alternatively spliced transcripts, and may act as an RNA. Dev. Dynam. *212*, 214–228. https://doi.org/10.1002/(sici)1097-0177(199806)212:2<214::Aid-aja6>3.0.Co;2-k.
79. Takahashi, N., Okamoto, A., Kobayashi, R., Shirai, M., Obata, Y., Ogawa, H., Sotomaru, Y., and Kono, T. (2009). Deletion of Gtl2, imprinted non-coding RNA, with its differentially methylated region induces lethal parent-origin-dependent defects in mice. Hum. Mol. Genet. *18*, 1879–1888. https://doi.org/10.1093/hmg/ddp108.
80. Yao, C., Yuan, Q., Niu, M., Fu, H., Zhou, F., Zhang, W., Wang, H., Wen, L., Wu, L., Li, Z., and He, Z. (2017). Distinct Expression Profiles and Novel Targets of MicroRNAs in human spermatogonia, pachytene spermatocytes, and round spermatids between OA patients and NOA patients. Mol. Ther. Nucleic Acids *9*, 182–194. https://doi.org/10.1016/j.omtn.2017.09.007.
81. Procópio, M.S., de Avelar, G.F., Costa, G.M.J., Lacerda, S.M.S.N., Resende, R.R., and de França, L.R. (2017). MicroRNAs in Sertoli cells: implications for spermatogenesis and fertility. Cell Tissue Res. *370*, 335–346. https://doi.org/10.1007/s00441-017-2667-z.
82. Zhao, L., Yao, C., Xing, X., Jing, T., Li, P., Zhu, Z., Yang, C., Zhai, J., Tian, R., Chen, H., et al. (2020). Single-cell analysis of developing and azoospermia human testicles reveals central role of Sertoli cells. Nat. Commun. *11*, 5683. https://doi.org/10.1038/s41467-020-19414-4.
83. Chen, S., An, G., Wang, H., Wu, X., Ping, P., Hu, L., Chen, Y., Fan, J., Cheng, C.Y., and Sun, F. (2022). Human obstructive (postvasectomy) and nonobstructive azoospermia - Insights from scRNA-Seq and transcriptome analysis. Genes Dis. *9*, 766–776. https://doi.org/10.1016/j.gendis.2020.09.004.
84. Malcher, A., Rozwadowska, N., Stokowy, T., Jedrzejczak, P., Zietkowiak, W., and Kurpisz, M. (2013). The gene expression analysis of paracrine/autocrine factors in patients with spermatogenetic failure compared with normal spermatogenesis. Am. J. Reprod. Immunol. *70*, 522–528.
85. World Health, O., and World Health, O. (2010). WHO Laboratory Manual for the Examination and Processing of Human Semen, 5th edn (World Health Organization).
86. Michaelis, M., Sobczak, A., and Weitzel, J.M. (2014). In vivo microinjection and electroporation of mouse testis. J. Vis. Exp. 51802. https://doi.org/10.3791/51802.

STAR★METHODS

KEY RESOURCES TABLE

REAGENT or RESOURCE	SOURCE	IDENTIFIER
Antibodies		
PARP	Cell Signal Technology	#9542
caspase-3	Cell Signal Technology	#9662
Beclin-1 (D40C5)	Cell Signal Technology	#3495
LC3A/B (D3U4C)	Cell Signal Technology	#12741
ERK	HuaBio	ET1610-13
p-ERK	HuaBio	ET1601-29
mTOR	Cell Signal Technology	#2983T
p-mTOR	Cell Signal Technology	#5536T
PCNA	Cell Signal Technology	#13110
p-NFκB	Cell Signal Technology	#3039
NF-κB	Cell Signal Technology	#8242
SPRY1	Bioss	bs-11216R
AGO2	Abcam	#ab57113
Bacterial and virus strains		
AAV9-MEG3-EGFP	Genechem	GOSV0278652
GFP-mCherry-LC3 lentivirus	Genechem	N/A
Biological samples		
Human testicular tissues	The first affiliated hospital of Zhengzhou University	N/A
Chemicals, peptides, and recombinant proteins		
3-MA	MCE	HY-19312
MEK162	MCE	HY-15202
IMD0354	MCE	HY-10172
Critical commercial assays		
mir VanaTM miRNA isolation kit	Ambion	Cat# AM1561
Agilent Bioanalyzer 2100	Agilent Technologies	N/A
Illumina HiSeq2500 Analyzer	Illumina	N/A
SimpleChIP Enzymatic Chromatin IP Kit	Cell Signal Technology	#9003
In Situ Cell Death Detection Kit	Vazyme	A113-01/02/03
Streptavidin Magnetic beads	Thermofish	#8816
Cell Counting Kit-8 (CCK-8)	Solarbio	#CA1210
Magna RIP kit	Millipore	#17-700
Annexin V Apoptosis Detection Kit	Vazyme	#A211
Deposited data		
Raw and analyzed data	This paper	GSE241326
Human reference genome NCBI build 37, GRCh37	Genome Reference Consortium	http://www.ncbi.nlm.nih.gov/projects/genome/assembly/grc/human/
miRNA expression profiling	Malcher et al.[84]	GEO database: GSE45887

(*Continued on next page*)

Continued

REAGENT or RESOURCE	SOURCE	IDENTIFIER
Experimental models: Cell lines		
Human NTERA-2 cells	The Cell Research Center, Institute of Basic Medical Sciences, CAMS/PUMC	N/A
Experimental models: Organisms/strains		
Mouse: 4-week-old ICR mice	Beijing Vital River Laboratory Animal Technology Co., Ltd	(ZZU-LAC20220114[04]
Oligonucleotides		
siRNA targeting sequence: si-MEG3-1:GGAUGGCACUUGACCUAGA	Genepharma	N/A
siRNA targeting sequence: si-MEG3-2: GGUUAAGUCUCUUGAAAGA	Genepharma	N/A
siRNA targeting sequence: si-SPRY1-1: GACCAGAUCAAGGCCAUAATT	Genepharma	N/A
siRNA targeting sequence: si-SPRY1-2: CCUGGUCAUAGGUCUGAAATT	Genepharma	N/A
The biotinylated MEG3	Genepharma	N/A
MEG3 FISH probe	RiboBio	N/A
Recombinant DNA		
pcDNA3.1-MEG3	Synbio technologies	N/A
psiCHECK™ -2	Promega	C8021
pRL-TK	Promega	E2241
pGL3-basic	Promega	N/A
pcDNA3.1-SPRY1	pcDNA3.1-MEG3	N/A
Software and algorithms		
miRDB	www.mirdb.org	
Starbase	https://starbase.sysu.edu.cn/starbase2/	
TargetScan	www.targetscan.org	
PROMO	https://alggen.lsi.upc.es/cgi-bin/promo_v3/promo/promoinit.cgi?dirDB=TF_8.3	
TFDB	http://bioinfo.life.hust.edu.cn/HumanTFDB#!/	
GTRD	http://gtrd.biouml.org/#!	
lncBase v3	http://bicresources.jcbose.ac.in/zhumur/lncrbase/	
miRcode	http://www.mircode.org/	

EXPERIMENTAL MODEL AND STUDY PARTICIPANTS

Testicular tissues

A total of 30 testicular tissue samples including 14 NOA and 16 control samples were obtained from men undergoing testicular puncture for IVF or ICSI at the First Affiliated Hospital of Zhengzhou University. All patients enrolled in the study were aged between 22 and 45 years. Testicular tissues of NOA group were obtained from testicular puncture of NOA patients undergoing intracytoplasmic sperm injection (ICSI) at the Reproductive Medicine Center, and testicular tissues of normal spermatogenic function(control) were obtained from testicular puncture of male patients due to sperm retrieval failure on the day of oocyte retrieval. Table 1 listed the demographic characteristics of the participants. Azoospermia diagnosis was based on the WHO fifth edition guidelines (2010).[85] When patients met the following criteria: (1) Absence of mature sperm in seminal fluid and sediment three times after centrifugation and inverted microscope screening; (2) B-ultrasound examination excluded the blockage of the vas deferens and retrograde ejaculation. (3) Testicular biopsy showed that there were no sperm or only a small amount of sperm, or spermatogenic cells were completely missing, and spermatogenic epithelium was composed only of Sertoli cells, the condition can be regarded as NOA. The patients met any of the following criteria were ruled out from the NOA group: (1) Patients aged less than 22 or over 45 years (2) No spermatozoa sampled with TESE. (3) Undescended testicles. (4) Chromosomal diseases, Cystic Fibrosis, Klinefelter syndrome, Leukocytospermia. (5) Patients receiving chemotherapy or radiotherapy. (6) History of mumps or orchitis. All patients

with NOA were diagnosed after a complete medical history and physical examination including scrotal ultrasound. This study was approved by the Ethics Committee of the First Affiliated Hospital of Zhengzhou University (2019-KY-78), and informed consent was obtained from each participant.

Microinjection of virus particles

This study constructed an adeno-associated virus (AAV9) that overexpressed the mouse homologous gene of human MEG3 and carried out seminiferous tubule microinjection to improve infection efficiency. The AAV9 virus was conducted by Genechem, Shanghai. AAV9 virus was injected into the seminiferous tubules through the efferent duct of 4-week-old ICR mice. The mice were randomly divided into two groups. The experimental group (E) was injected with AAV9-MEG3-EGFP; the control group (C) was injected with AAV9-NC-EGFP. The glass capillaries were pulled to 50 μm in diameter using a vertical capillary puller as the microinjection needle. A 10 μL virus particles compound with 0.04% Trypan blue solution (Sigma-Aldrich) was loaded into the microinjection needle. Consequently, the microinjection needle was connected to the micromanipulator/injector unit. After the mice were anesthetized, an incision was made in the middle of the abdomen. We carefully pulled up the fat pad in the abdomen to expose the attached testicle, located the output tubule, and placed it on a sterile paper tape to ensure clear visibility of the output tubule. The microinjection needle was placed parallelly to the output tubule, with the tips pricking the efferent duct toward the rete testis and stopped just as it penetrated the rete testis. Virus solutions were injected through a micromanipulator with the following settings: pi: 100 hPa, ti: 0.2 s, and pc: 0 hPa.[86] And the filling state of the testis was observed with blue color to monitor the entire injection process. After the injection was complete, the testicles were returned to the abdominal cavity. The abdominal incision was sutured, the mice were placed on the warm pad until waking up, and the microinjection was completed. All mice were sacrificed, and the testes were removed for further experiment seven days after injection. All animal work was performed with the approval of the Research Ethics Committee of Zhengzhou University (ZZU-LAC20220114[04]).

METHOD DETAILS

RNA purification, RNA-Seq library construction and sequencing

Three NOA and corresponding control testicular biopsy specimens for RNA-seq analysis were filtered out according to the above standard. Testicular tissues were washed three times with phosphate-buffered saline (PBS) immediately after retrieval and stored in liquid nitrogen until use. Total RNA was extracted using mir VanaTM miRNA isolation kit (Cat# AM1561, Ambion) following the instructions of the manufacturer and checked for a RIN number to inspect RNA integrity using an Agilent Bioanalyzer 2100 (Agilent Technologies, Santa Clara, CA, US). Qualified total RNA was further purified using RNAClean XP Kit (Cat A63987, Beckman Coulter, Inc. Kraemer Boulevard Brea, CA, USA) and RNase-Free DNase Set (Cat#79254, QIAGEN, GmBH, Germany). The RNA-seq criteria required a minimum RIN $\geq$7.0 for each sample to be qualified. For library preparation, rRNA removal, RNA fragmentation, first-strand cDNA synthesis, second-strand cDNA synthesis, end-repair, and adapter ligation were performed following standard protocols. The library fragments were measured using a Qubit 2.0 Fluorometer to select cDNA fragments of preferentially 350 bp in length. Moreover, Agilent 2100 was used to assess library quality. Sequencing was performed using an Illumina HiSeq2500 Analyzer (Illumina, San Diego, CA, USA) according to the manufacturer's protocol. Data filtering and analysis were controlled by Illumina's Data Collection software. The reads were mapped with the Spliced Mapping algorithm Hisat2 (Version: 2.0.4) for sequence alignment on GRCh38 (hg38) reference.

Cell lines and cell culture

The human NTERA-2 cell (NT-2) lines was obtained from the Cell Research Center, Institute of Basic Medical Sciences, CAMS/PUMC (Beijing, China). Cells were cultured in a humidified incubator under a 5% CO2 atmosphere at 37 °C in Dulbecco's modified Eagle's medium (DMEM) supplemented with 10% fetal bovine serum (FBS) (Pricella, China) and 100 U/ml penicillin/streptomycin (BI, USA).

Plasmid construction and cell transfection

To overexpress MEG3 and SPRY1, the full-length MEG3 (NR_002766.2) and SPRY1 (NM_001258038.2) cDNA fragments were synthesized by Synbio Technologies (Suzhou, China) and cloned into the pcDNA 3.1 (+) plasmid. The empty pcDNA3.1(+) vector was used as the control. EcoRI and XhoI were used for the cloning of MEG3, NheI and EcoRI were used for the cloning of SPRY1. To knockdown MEG3 and SPRY1, small interfering RNA (siRNA)-MEG3 (si-MEG3) and si-SPRY1 were designed and synthesized by GenePharma (Shanghai, China). The sequence of siRNAs were listed in Table S1. A scramble siRNA was used as negative control (si-NC). The miRNA double-stranded miR-21 mimics, inhibitor and the corresponding negative controls were synthesized by GenePharma. The human NT-2 cells were transfected with siRNAs or plasmid using Lipofectamine 3000 Transfection Reagent (Invitrogen), according to the manufacturer's instructions. The transfection efficiency was determined by qPCR. The transfection efficiency was determined by qPCR and Western blot as shown in the corresponding figures. The knock-down efficiency of siRNA was more than 70%. The overexpression efficiency of MEG3 or SPRY1 was more than 3 times.

Reverse transcription and quantitative real-time PCR (qPCR)

Total RNA was extracted from cells or tissues using TRIzol reagent (Takara). RNA was reversely transcribed using PrimeScript RT Master Mix (AG, China). For miRNA reverse transcription, we used the stem-loop method by adding an additional reverse transcription primer. cDNAs

were quantified using SYBR Premix Ex Taq (Takara, Japan) on ABI7500 instrument. Primers using in RT-qPCR were listed in Table S2. Relative quantification was determined using the 2-ΔΔCt method. Expression of miR-21 was normalized to U6. Expressions of MEG3 and mRNA were normalized to β-actin. All results were performed independently in triplicate.

Western blot

NT-2 cells or mouse testicular tissues were collected and lysed using RIPA protein extraction reagent (Beyotime, Beijing) with protease inhibitor cocktail and phosphatase inhibitor cocktail (Selleck, Shanghai). Equal amount of protein in homogenate samples were separated in SDS-PAGE (Bio-Rad) and transferred to polyvinylidene difluoride (PVDF) membranes (Millipore, MA, USA). After blocked with 5% non-fat milk, the membranes were incubated with the anti-rabbit PARP, caspase-3 (1:1000 dilution, Cell Signal Technology), anti-rabbit Beclin-1 (D40C5) (#3495, Cell Signal Technology) and LC3A/B (D3U4C) (12741, Cell Signal Technology), SPRY1 antibodies (bs-11216R, Bioss, China), ERK and *p*-ERK antibodies (ET1610-13 and ET1601-29, HuaBio, China), and mTOR (2983T, Cell Signal Technology) and *p*-mTOR antibodies (5536T, Cell Signal Technology) at 4 °C for 12 h. Mouse antihuman antibodies GAPDH (1:5000 dilution; FD) was used as a loading control. Followed by washing with phosphate buffer solution (0.1%) containing Tween 20, the membranes were incubated with horseradish peroxidase-labeled goat anti-rabbit IgG (1:10000) or goat anti-mouse IgG (1:10000) for 1h. The images were obtained by Amersham Imager 600 and the gray values were analyzed with ImageJ software.

Immunohistochemical (IHC) staining

Immunohistochemistry (IHC) was used to measure the expression of PCNA and SPRY1 in mouse testicular tissues. Briefly, the 4-μm thickness sections were deparaffinized in xylene and rehydrated using graded ethanol. Afterward, sections were incubated with 3% H_2O_2 for 10 min followed by 10% normal goat serum for 15 min at room temperature to block endogenous peroxidases. Then, the sections were successively incubated with the primary antibody at 4 °C overnight and the horseradish peroxidase (HRP)-labeled secondary antibody at 37 °C for 20 min. After counterstaining with hematoxylin, the sections were observed under an microscope (Nikon Corporation, Tokyo, Japan).

Heamatoxylin and eosin

(H&E) staining was performed to evaluate the morphological changes of testicular tissues from mice. Briefly, the 4-μm paraffin-embedded mouse testicular tissues sections were subjected to H&E staining and captured under an Olympus microscope.

FISH

The localization of MEG3 in human testis and NT-2 cells were assessed by lncRNA FISH probe mix and matching kits (RiboBio, Guangdong, China). The specific probe of MEG3 was synthesized by RiboBio, Guangdong, China. For NT-2 cells, 3×10^3 cells/well were seeded into 24-well and incubated for 24h. The samples (cells or tissues) were fixed by 4% paraformaldehyde, permeated with 0.5% Triton X-100, blocked by prehybridization solution at 37°C, and then incubated with MEG3 probe at 37°C overnight. After staining with DAPI, the images were captured using a confocal laser scanning microscope (ZEISS).

Bioinformatic prediction

miRcode and LncBase (Maria D. et al., 2016; Data ref: Maria D. et al., 2016) were used to seek the potential target gene for MEG3. miRNAs overlapped in the two databases were selected for further study. ViennaRNA Web Services were used to predict the binding site of MEG3 with miR-21. miRDB, Starbase and TargetScan were used to select the target gene and binding sites for miR-21. PROMO, TFDB and GTRD database were used to predicted the potential transcription factors of MEG3.

RNA-seq of testicular biopsy specimens of 16 patients with non-obstructive azoospermia (NOA) and 4 with normal spermatogenesis was obtained from GSE45887 cohort in the GEO database. Single-cell RNA sequencing of five normal adult samples and iNOA (3 cases) were obtained from GSE149512. Single-cell RNA sequencing of normal fertility samples were obtained from GSE106487.

RNA immunoprecipitation assay

The RIP assay was conducted using Magna RIP kit (Millipore) according to the manufacturer's instructions. Briefly, Protein G magnetic beads were conjugated with AGO2 antibody (#ab57113, Abcam, Cambridge, MA, USA) or negative control mouse IgG (Millipore, Bedford, MA, USA). Then, cells were lysed in RIP lysis buffer and incubated with magnetic beads. After being washed, the beads were cultured with proteinase K to digest proteins. The immunoprecipitated RNA was extracted by Trizol reagent (Takara) and detected by qRT-PCR.

RNA pull-down assay

The biotinylated MEG3 was obtained from GenePharma (Shanghai, China). Briefly, streptavidin magnetic beads were used to captured biotinylated probe. After fixed with formaldehyde to cross-link RNA, the NT-2 cells were lysed and incubated with the magnetic beads attached with the probe. Finally, the RNA–RNA complexes were purified using Trizol reagent (Takara). Expression of miR-21 was detected by RT-qPCR.

Cell counting kit-8 assay

Cell counting kit-8 was performed to determine the cell vitality. Briefly, $2x10^3$ NT-2 control or treated cells were seeded in 96-well plate. CCK-8 solution was mixed in DMEM culture medium and then incubated with cells at specified time points for 4h. Optical density at 450 nm (OD450) was recorded for each sample using a full wavelength microplate analyzer (Molecular Device).

EDU assay

The DNA synthesis rate was evaluated using a 5-ethynyl-20-deoxyuridine (EdU) assay kit (Abbkine) following the manufacturer's instructions. Briefly, the transfected cells were seeded onto 96-well plates at a density of $2x10^4$ per well and cultured at 37°C with 5% CO_2 for 24 h. Then, the culture medium was replaced by serum-free medium blended with EDU for 2h incubation. After counterstaining with DAPI, the fluorescences were observed and imaged by an inverted fluorescence microscope (Olympus, Tokyo, Japan) at 100× magnification. The cell proliferation activity was evaluated by the ratio of EdU-stained cells (with red fluorescence) to Hoechst-stained cells (with blue fluorescence).

Flow cytometry

A FITC Annexin V Apoptosis Detection Kit (Vazyme, China) was used to detect cell apoptosis. The transfected cells were trypsinized and washed with cold PBS twice. After resuspending in 100 μL binding buffer, the cells were staining with 5 μL Annexin-V-FITC and 5μL PI for 10 min. Flow cytometry analysis (FACS Calibur, BD Biosciences, San Jose, CA, USA) was performed within 30 min after staining. The apoptotic cells concluded the right upper quadrant (late stage apoptotic cells) and the right lower quadrant (early apoptotic cells).

TUNEL

Mouse testicular tissues were collected and cut into 4 μm-thick sections. A terminal deoxynucleotidyl transferase-mediated dUTP nick end labeling (TUNEL) assay was detected using *In Situ* Cell Death Detection Kit (Vazyme). Images were observed under a fluorescence microscope.

ChIP assay

A SimpleChIP Enzymatic Chromatin IP Kit (CST) was used for the ChIP assay according to the manufacturer's protocol. JASPAR CORE database was used to identify the binding sites between NF-κB and the genomic region 2000 bp upstream of the MEG3 sequence. The obtained DNA was analyzed by qPCR using primers targeting the predicted binding sites. The primer sequences were listed in Table S3.

Dual luciferase reporter assay

Wild type (WT) of the MEG3 cDNA fragment containing the predictive binding site of miR-21 was cloned into the downstream of the Renilla psiCHECK2 vector (Promega, Madison, WI). The mutant (MUT) MEG3 containing the point mutations of the miR-21 binding site was specifically synthesized and inserted into the psiCHECK2 vector the same with the WT plasmid. To confirm the direct combination of miR-21 and SPRY1, wild-type (WT) and mutant (MUT) SPRY1 3′-UTR fragments were cloned into the psiCHECK2 vector (Promega) similarly. The above plasmids were synthesized by Synbio Technologies (Suzhou, China). The WT or Mut plasmids were co-transfected with miR-21 mimics or mimic controls by Lipofectamine 3000 in NT-2 cells. Wild type of the sequence of primer3 in the chip assay was cloned into the pGL3-Basic vector (Promega, Madison, WI). The mutant binding site as shown in Figure 7E was specifically synthesized and inserted into the pGL3-Basic vector the same with the WT plasmid. Wild-type(WT) or mutant(MUT) transcription plasmids and the pRL-TK plasmid (Standard Renilla luciferase) were co-transfected by in NT-2 cells treated with IMD0353 or DMSO.

After 48 h of transfection, the renilla and firefly luciferase activity were detected by the Dual-Luciferase Reporter Assay System (#E2920, Promega).

Immunostaining

Cells or mouse testicular tissues were permeabilized with 1% Triton X-100 and then blocked with 5% BSA. After stained with LC3A/B antibody (CST) at 4°C overnight, the samples were incubated with Cy3-conjugated FITC-conjugated goat-*anti*-rabbit secondary antibody (Millipore, Billerica, MA) for 1 h at room temperature. DAPI was used to stain Nuclei for 5 min. Fluorescence signals were observed with a confocal fluorescence microscopy (Leica Microsystems, Germany).

GFP-mRFP-LC3 lentivirus transfection and confocal microscopy

GFP-mRFP-LC3 lentivirus was synthesized by Genechem, Shanghai. In short, shuttle plasmid, pHelper 1.0 vector plasmid and pHelper 2.0 vector plasmid were transfected into HEK293T cells, and then cellular supernatant was collected 24 h and 48 h after transfection and stored at 4°C. The collected supernatant was passed through the tangential flow filtration system. To concentrate virus, The samples were purified by AKTA Canal-cation chromatography system. Virus titer was detected by absolute quantitative method. NT-2 cells were infected with GFP-mRFP-LC3 lentivirus particles at ten multiplicities of infection (MOI). At 48 h after transduction, cells were screened with puromycin at 2 μg/mL. Stably transfected cells were inoculated in the confocal dish for further transfection. Appropriate time after treatment, cells were

fixed with 1 mL of 4% paraformaldehyde for 30 min and then washed with PBS three times. Fluorescence images were collected with a laser-scanning confocal microscope. Autophagic flux was determined by counting the fluorescent puncta of yellow and red dots.

QUANTIFICATION AND STATISTICAL ANALYSIS

Data are presented as described in the figure legends. All of the statistical details of experiments can be found in the figures and figure legends. Data analysis of RNA-seq were described in STAR Methods. The numbers of clinical testicular tissues were provided in Table. A chi-square test was performed to analyze clinicopathological characteristics. Spearman correlation coefficient was used to evaluate correlations. The numbers of animals undergoing seminiferous tubule microinjection were descripted in legend of Figure 2. Student's t test was used to analyze expression differences and *p* values were calculated using GraphPad Prism. Standard deviation (SD) is represented in results by error bars. Multiple comparisons were conducted by one-way ANOVA. GraphPad Prism 9.0 (La Jolla, CA) and SPSS 20.0 (SPSS, USA) were used to conduct statistical analyses. *p* values were represented in figures combined with figure legends, less than 0.05 were considered statistically significant.